UPPSALA
UNIVERSITET

Digital Comprehensive Summaries of Uppsala Dissertations from the Faculty of Science and Technology 1671

Aerodynamic Studies of Vertical Axis Wind Turbines using the Actuator Line Model

VICTOR MENDOZA

ACTA
UNIVERSITATIS
UPSALIENSIS
UPPSALA
2018

ISSN 1651-6214
ISBN 978-91-513-0338-3
urn:nbn:se:uu:diva-348346

Dissertation presented at Uppsala University to be publicly examined in Häggsalen, Ångströmlaboratoriet, Lägerhyddsvägen 1, Uppsala, Tuesday, 5 June 2018 at 09:00 for the degree of Doctor of Philosophy. The examination will be conducted in English. Faculty examiner: Senior researcher Robert Flemming Mikkelsen (Technical University of Denmark).

Abstract
Mendoza, V. 2018. Aerodynamic Studies of Vertical Axis Wind Turbines using the Actuator Line Model. *Digital Comprehensive Summaries of Uppsala Dissertations from the Faculty of Science and Technology* 1671. 85 pp. Uppsala: Acta Universitatis Upsaliensis. ISBN 978-91-513-0338-3.

This thesis addresses the unsteady aerodynamics involved in the operation of vertical axis wind turbines (VAWTs). The main focus is to represent and understand the most relevant phenomena within the resulting flow pattern as the wake structure, loads on the different turbine components and the performance of the rotor. An actuator line model has been used for this purpose.

This model has been validated against experimental measurements from diverse cases with different operating conditions in both confined wind tunnels and open site locations. Numerical works were carried out considering a wide range of tip speed ratios (TSRs), and therefore covering from the no stall to the deep stall regime. The latter requires the implementation of a dynamic stall model for the proper representation of the unsteady forces on the blades. Also, different inlet conditions such as a uniform flow, a logarithmic wind shear and an atmospheric boundary layer (ABL) have been tested. The so-called recycling method technique was used to produce the fully developed ABL flow. Additionally, the resulting wake and performance of interacting turbines has been studied.

Once the model was validated, two numerical study cases for large scale turbines were carried out. First, the performance and resulting flow field from both a horizontal axis wind turbine (HAWT) and VAWT were investigated when the turbines were operating at their optimal TSR and within the same ABL inflow boundary conditions. The influence of the variation on the atmospheric turbulence levels was also studied, as well as the differences and similarities on the obtained results for both type of turbines. Later, the performance improvement of two interacting VAWTs was investigated through the deflected wake produced by the pitched struts of the upstream turbine. This is presented as a novel mechanism to mitigate losses on interacting turbine arrangements (i.e. wind farms).

In general, there is a reasonable good agreement between numerical results and experimental measurements, and therefore, the applied ALM can be considered as a potential tool for VAWTs simulations, characterized by relatively low computational cost showing accuracy and numerical stability.

Keywords: wind power, vertical axis wind turbines (VAWTs), actuator line model (ALM), dynamic stall model (DSM), atmospheric boundary layer (ABL), wake deflection, atmospheric boundary layer (ABL)

Victor Mendoza, Department of Engineering Sciences, Electricity, Box 534, Uppsala University, SE-75121 Uppsala, Sweden.

ISSN 1651-6214
ISBN 978-91-513-0338-3
urn:nbn:se:uu:diva-348346 (http://urn.kb.se/resolve?urn=urn:nbn:se:uu:diva-348346)

To Goedele Verburgh

"Nothing really matters, anyone can see
nothing really matters to me... any way the wind blows"
-Queen

List of papers

This thesis is based on the following papers, which are referred to in the text by their Roman numerals.

I **Mendoza, V.,** Bachant, P., Wosnik, M., Goude, A., "Validation of an Actuator Line Model Coupled to a Dynamic Stall Model for Pitching Motions Characteristic to Vertical Axis Turbines", *In "Proceedings of The Science of Making Torque from Wind, TORQUE 2016" Munich, Germany,* October 2016

II **Mendoza, V.,** Goude, A., "Wake Flow Simulation of a Vertical Axis Wind Turbine Under the Influence of Wind Shear", *In "Proceedings of the Wake Conference 2017" Visby, Sweden,* June 2017

III **Mendoza, V.,** Bachant, P., Ferreira, C., Goude, A., "Near-Wake Flow Simulation of a Vertical Axis Turbine Using an Actuator Line Model", *Submitted to Wind Energy,* April 2018

IV **Mendoza, V.,** Goude, A., "Validation of an Actuator Line and Vortex Model using Normal Forces Measurements of a Straight-Bladed Vertical Axis Wind Turbine", *Submitted to Renewable Energy,* April 2018

V **Mendoza, V.,** Chaudhari, A., Goude, A., "Performance and Wake Comparison of Horizontal and Vertical Axis Wind Turbines Under the Influence of the Atmospheric Boundary Layer", *Submitted to Wind Energy,* April 2018

VI **Mendoza, V.,** Goude, A., "Improving Farm Efficiency of Interacting Vertical Axis Wind Turbines Through Wake Deflection Using Pitched Struts", *Submitted to Wind Energy,* April 2018

Contents

Nomenclature

Symbol	**SI-unit**	**Description,** where $n = 0, 1, 2, 3...$
A	m^2	Turbine cross-sectional area
A_n	-	Fourier coefficient
C_D	-	Drag coefficient
C_{D0}	-	Drag coefficient at zero angle of attack
C_L	-	Lift coefficient
C_N	-	Normal force coefficient
C_N^f	-	Normal force coefficient for trailing edge separation
C_N^v	-	Normal force coefficient during vortex convection
C_T	-	Tangential force coefficient
D_f	-	Deficiency function for separation point
D_α	-	Deficiency function for geometrical angle of attack
E_0	-	Constant for tangential force coefficient
Ω	rad/s	Rotational speed of a turbine
F_D	N	Drag force
F_L	N	Lift force
F_N	N	Normal force
F_T	N	Tangential force
K	-	Von-Kármán constant
N_B	-	Number of turbine blades
P	W	Absorbed power by a turbine
P_{wind}	W	Total power available in a wind flow
Q	Nm	Absorbed torque by a turbine
S_1, S_2	-	Coefficients for separation point
T	N	Thrust of the turbine rotor
T_f	-	Empirical time constant for dynamic separation point
T_α	-	Empirical time constant for delay in pressure response
V	m/s	Flow velocity
V_{blade}	m/s	Blade velocity
V_{in}	m/s	Local incoming flow velocity
V_{rel}	m/s	Relative flow velocity
V_∞	m/s	Asymptotic wind velocity
X, Y, Z	-	Deficiency functions for unsteady attached flow
c	m	Blade chord length

Symbol	SI-unit	**Description,** where $n = 0, 1, 2, 3...$
d	m	Arbitrary distance from the quarter chord position
f	-	Static flow separation point
f'	-	First-order delayed flow separation point
f''	-	Dynamic flow separation point
g	m/s^2	Gravitational acceleration
k	-	Reduced frequency of a pitching blade
m	kg	Mass of the blade with support arms
q_0	-	Critical reduced pitch rate
q_n	-	Reduced pitch rate
r	m	Turbine radius
Δs	-	Non-dimensional time-step
t	s	Time
x_0	-	Normalized blade attachment point
Γ	m^2/s	Total two-dimensional circulation of a blade
α	-	Angle of attack
α'	-	Delayed angle of attack due to pressure delay
$\dot{\alpha}$	rad/s	Blade pitch rate
α_I	-	Angle of attack for a breakpoint of flow separation
α_{cr}	-	Critical angle of attack
α_{ds0}	-	Critical stall onset angle
α_{ss}	-	Static stall onset angle
γ	-	Blade pitch angle
ε	m	Force smoothing width parameter
η	-	Efficiency factor for tangential force coefficient
η_F	-	Force smoothing function
θ	-	Blade azimuth angle
$\hat{\theta}$	-	Unit vector in the tangential direction
λ	-	Tip speed ratio
ν	m^2/s	Kinematic viscosity
ρ	kg/m^3	Air density
φ	-	Angle of relative flow velocity
z_0	m	Roughness length

Abbreviations

Abbreviation	Description
ALM	Actuator line model
BEM	Blade element model
CFD	Computational fluid dynamics
DSM	Dynamic stall model
HAWT	Horizontal axis wind turbine
LES	Large eddy simulation
NACA	National Advisory Committee for Aeronautics
TSR	Tip speed ratio
VAWT	Vertical axis wind turbine

1. Introduction

A wind turbine is a device which extracts the kinetic energy from the atmospheric wind flows, converting it into a torque on the rotor, which is connected to the main shaft and spins a generator to create electricity. These devices can be divided mainly into two groups: horizontal and vertical axis types. This thesis comprises the study of the aerodynamics of vertical axis wind turbines (VAWTs) using the actuator line model (ALM) approach. The main focus is to represent and understand the most relevant phenomena involved in the resulting flow pattern as the wake structure, loads on the different components and the performance of the device for different operating conditions. Additionally, horizontal axis wind turbine (HAWT) cases have been tested in order to evaluate the performance of the presented model on these devices and for a comparison against vertical axis turbines.

1.1 A historical perspective of wind energy

1.1.1 Vertical axis windmills

The first vertical windmills were founded in the Orient, according to historians. It is said that around 1700 B.C., Hammurabi used windmills for watering the plains of Mesopotamia. Written evidence reveals an early use of wind power in Afghanistan, moreover, documentation from 700 A.D. confirms that millwright was considered an occupation of high social esteem over there [1]. Nowadays, is still possible to find in Iran and Afghanistan ruins of these windmills that were operating for centuries (see figure 1.1).

The oldest windmills found were employed by Persians and they were built with a vertical axis of rotation. Braided mats were attached to a rotating axis, and therefore, driven by drag forces along with the wind. The Persian windmills were characterized by asymmetry since half of the rotor was screened with a wall.

The Chinese windmills (approx. 1000 A.D.), also built with a vertical axis, used the braided mats as sails with no screening wall and therefore they had the typical advantage of vertical axis windmills for omni-directionality which allows them to operate with winds from any direction.

The simplicity of the design and construction of vertical axis devices allowed to attach a power extraction component (pump, millstone, etc.) directly to the rotating shaft with no requirement of redirecting the rotational movement and/or intermediate gears. Advanced "Occidental" versions of vertical

Figure 1.1. The Neshtifan (Iran) windmills, built sometime between 500 to 900 A.D. Image taken from [2].

axis principle used, partially or totally, the lift force as driving force. This will be discussed in detail in the section 1.2.

1.1.2 Horizontal axis windmills

In the Occident, very much later, a wind turbine type different from the Oriental vertical axis version was developed. The main variation on the design is the horizontal axis whose sails (blades) rotate in a vertical plane perpendicular to the ground and the incoming wind, just like a propeller. A new principle is introduced with this turbine type, since the sails are not obstructing the flow in order to produce the necessary drag forces for the rotor operation, then, these devices were characterized by a lift-driven horizontal axis.

The first approach to a theoretical description of the lift force on blades dates only of one century ago, however, these devices were mentioned or already built in England from the 12th century and it was called the post windmill, which main characteristic is that it has a whole body (mill house) where the machinery mounted on a vertical central post inside, around which and it can be turned and oriented into the wind. Besides the waterwheel, the post mill was the most important driving engine, hence, it spread from England and France to Russia (via Holland, Germany and Poland) during the 13th and 14th centuries. It is not well defined between historians who invented it and where it came from, anyway, it seems to be a general agreement the Crusaders brought the wind mill concept from Persia and Middle East [3] (see figure 1.2).

It is only since 19th century when two lantern gears were implemented on post windmills for operating two sets of millstones in parallel. The post windmill has been used exclusively for grinding grain.

In Holland, at the 15th century, a strong economic interest came in the reclamation of lands by draining the polders, hence, it brought the first attempts to

Figure 1.2. Brill windmill, a 17th Century post mill in Buckinghamshire. Image taken from [4].

drive pumps by using wind energy. The post windmill had to be modified for this goal since the pump was located under the mill, and therefore, the driving power had to be transmitted there. By using a gearbox inside the revolving mill house together with an archimedean screw (or a scoop wheel) placed below a pyramidal-shaped structure this machine could achieve the required drainage purposes, resulting in the so-called wipmolen. Later, this principle was also applied in the construction of grain mills due to the advantage given by this configuration with no need of carrying up and down heavy loads (e.g. mill-stones, sacks of grain and flour) in the mill house [5].

In Southern Europe, post mills did not reach a considerable popularity. A different windmill version was widely spread there, the so-called tower mill, which consists in a cylindrical mill house made of stone, a thatched roof and a multi-sails (eight or more) driven rotor. These machines were early used for irrigation and their first documentation dates from the 13th century [1]. A modified latter versions (principally in the south of France) had a turnable wood-made cap and four sails (blades) driven rotor as the post windmills (see figure 1.4).

The turnable cap is the main feature of the Dutch smock mill which became popular in the 16th century. It is a modified version of the tower mill since the wooden structure of the tower is lighter than the heavy stone construction of the tower mill, which could be easier raised on the wet and muddy lands of Holland where their principal use was for drainage of the polders, while in the rest of Europe, mainly for grinding grain. In the Netherlands, with around ten thousands of Dutch smock mills built between the 18th and 19th century, the use of wind energy experienced its peak, and even more, this leads to a standardization of its construction which was totally unusual for that period.

An exotic development of the 17th century, the Paltrock windmill, demonstrated that wind energy can be employed universally as a driving force. The

Figure 1.3. Stembridge Tower Mill, in High Ham, Somerset. Image taken from [6].

entire mill rested on a live ring in such a way that an whole sawmill was driven by a wind wheel.

The last relevant development occurred in the middle of the 19th century with the Western mill, which was mainly employed to provide drinking water for both humans and farm beasts on North America. Its main feature of this kind of device is the rotor rosette with more than twenty metal sheet blades and a rotor diameter between 3 m and 5 m. The rotor is located at the top of a metal lattice tower and it employs a crankshaft to drive a piston pump.

Figure 1.4. American windmill. Alde Feanen. Image taken from [7].

1.2 Modern vertical axis wind turbines

In this thesis, as it was already mentioned, a wind turbine is defined as an energy converter. Independent of its application, type of details on the design it transforms the kinetic energy from the atmospheric wind into mechanical ro-

tational energy and then into electricity by using an electrical generator, while the windmill only gives mechanical power as an output.

Nowadays, the most conventional design of wind turbine is the horizontal axis turbine (HAWT), where the rotation axis is parallel to the ground [8]. However, in this thesis the primary focus for investigation is on vertical axis turbines (VAWTs). Here, the rotational axis is perpendicular (normal) to the ground plane, these kind of turbines are sometimes called cross-flow turbines, since it can work even being rotated 90°, as long the flow is perpendicular to the rotor axis.

The lift and the drag-driven forces are the two main aerodynamic principles for classifying VAWTs. The latter type is commonly called Savonius type after being developed by the Finnish inventor Sigurd Johannes Savonius in the early 19th century resulting in two US patents documented in [9,10], although he only improved the existing drag turbines. It is one of the simplest turbines. Aerodynamically, it is a drag-driven rotor device which consists in two (or three) scoops. Looking from the top, a two-scoops configuration can look like an "S" in a cross-section with a gap in the middle. For every time, at least one of the scoops will operate in the same direction as the wind, while the remaining cup(s) will be moving against the wind experiencing less drag due to the curvature. The differential drag gives a torque on the turbine. In general, Savonius turbines have low efficiencies although power coefficients close to 0.3 have been measured [11]. Their efficiency is much less than the one given by other lift-based turbines of similar size. Another disadvantage of these turbines is the relatively large amount of construction material required restricting (mainly economically) their scalability for large scales, as it can be observed in figure 1.5.

Figure 1.5. Different types of vertical axis wind turbines: Savonius (left), Darrieus (middle) and H-rotor type (right). Images taken from [12–14], respectively.

Another type of VAWT is lift-driven based, the Darrieus turbine. Designed and patented by the French aeronautical engineer Georges Jean Marie Darrieus, the filing for the patent was the 1st of October, 1926 [15]. This tur-

bine consists of two or three curved blades with an airfoil profile in the cross-section and which are mounted on a vertical rotating shaft. The patent of Darrieus covers both curved and straight blades. The goal of the curved blades design is to mitigate bending stresses on blades due to centrifugal forces. The Darrieus turbine is more efficient than a Savoniuos one and it needs less construction material (see figure 1.5), however, its main drawbacks are the oscillating forces causing fatigue, turbine protection from extreme wind conditions and difficulties in self-starting. The most successful VAWT was developed in the early 1980s by the North American company Flowind, which installed more than 500 two-bladed turbines in California. However, there was a lack on the deeper understanding about blade fatigue at that time, resulting in serial failures in the joints between the sections of extruded aluminum blades, and therefore, fatigue and design weaknesses led to increasing unreliability and they were removed [1].

The presented thesis is focused on the straight blade H-rotor turbine type, which is under development at Uppsala University nowadays. Considering modern light materials, the turbine can be built using composites which reduce the centrifugal forces due to the lighter overall structure. Some advantages of the blades design are that straight blades are easier to manufacture, additionally, by attaching the blades with struts, it allows to locate the upper bearing closer to the turbine center reducing bending moments in the shaft. Also this type of turbine is characterized by a larger cross-section area (compared to curved blades) which is proportional to the power available. On the other hand, the disadvantages of straight-blade turbines are the need of additional struts and the presence of large bending moments on the blades produced by centrifugal forces.

The nowadays trend of wind energy industry aims for the development of large scale turbines in offshore environments [16–18], since it offers larger capacity factors with stronger and more consistent winds, lower levels of turbulence and less pronounced wind shears compared to onshore environments [19]. Even more, wind energy facilities onshore suffer relevant environmental impacts [20]. Under this scenario, a renewed interest in VAWTs has been brought, since the characteristics provide several advantages over the conventional HAWTs and their implementation can potentially reduce the new challenges the offshore environment hands out. Several European and North American projects have been focused on floating large scale VAWTs [21, 22]. VAWTs can work with winds from any direction (omni-directionality) which excludes the need of a yawing system and often the pitching mechanism, resulting in a simpler mechanical design with a few moving parts. This feature is highly appreciated since the yawing and pitching combined mechanisms account for a 33% of the failures [23] and considering that in offshore facilities

[1] http://www.wind-works.org/cms/index.php?id=64&tx_ttnews%5Btt_news%5D=2194&cHash=d1b21f3bd1f35d9e4804f1598b27bd86

the operation and maintenance have a large contribution in the total energy production cost. Another advantage of the VAWTs is the vertical orientation of the shaft allowing the generator to be placed at sea level, and thereby lowering the center of gravity and reducing the complexity of its installation and maintenance. Furthermore, concerns about the dimensions and weight of the generator are mitigated, favoring the installation of heavy direct drive generators with permanent magnets [24]. All these features for VAWTs show higher potential for scalability considering the operational inconveniences and limitations of HAWTs due to the yawing mechanism and the location of the generator.

The operation of VAWTs is naturally characterized by complex and unsteady aerodynamics, which poses considerable challenges to overcome by both measurements and numerical modeling [25]. Some aspects like theoretical and real aerodynamic efficiency of a stand-alone turbine or losses on farms due to wakes have not been properly undertaken yet. VAWTs are inherently exposed to cycling variation on the angle of attack, resulting in cyclic blades forces which can potentially generate material fatigue damage.

As long there is an increasing interest for the design and analysis of VAWTs, there will remain a need for overcoming the lack of understanding of the main physical phenomena involved in VAWTs aerodynamics and reliable numerical models to characterize it (unless it has been overcome).

1.3 Vertical axis wind turbines research at Uppsala University

Since 2002, wind power research has been conducted in the Division of Electricity at Uppsala University. During this period, three H-rotor turbines were built: a small one with a diameter of $D = 6$ m with rated of 1.5 kW, followed by a 10 kW rated turbine for telecom applications [26] and a rated power 12 kW [24, 27, 28]. The latter turbine has been used for the majority of the experiments. Later on, a large scale VAWT rated at 200 kW turbine was built by the spinoff company Vertical Wind AB in Falkenberg [29]. The research on these turbines have been carried out in eight doctoral theses [30–37] and the development of simulations tools were made by Dyachuk [35], Goude [33] and Deglaire [31].

1.4 Contribution of this thesis

The focus of this work has been on the modeling part of the main phenomena involved in the aerodynamics of VAWTs using the actuator line model (ALM) approach. Qualitative and quantitative analyses of the resulting flow pattern (wake), forces on blades and rotor performance of VAWTs have been carried

out. This unsteady model has been tested and validated in a wide range of different operational conditions.

Initially, the model was used to calculate the blade loading and body force of a pitching airfoil in similar operating conditions as an H-rotor type VAWT and it is published in Paper I. Later, it was studied the wake produced by a VAWT located in an open site and how it is affected by the surface roughness of the terrain, without considering the atmospheric turbulence, this study is published in Paper II. A further study of the near-wake generated for a VAWT within a wind tunnel facility is presented in paper III. Also, the presented ALM has been compared to a 2D and a 3D vortex model by representing the normal forces on a blade of an operating 12 kW VAWT which is located in an open site in the north of Uppsala (Sweden), and the results are published in Paper IV. All these mentioned works were validated using experimental measurements.

A numerical study of the influence of the atmospheric boundary layer (ABL) on large scale wind turbines is published in Paper V and the improvement of the farm efficiency with interacting VAWTs through wake deflection using pitched struts is published in Paper VI. The influence of the open jet inlet on the wind turbines experiments is published in Paper VII, for this purpose results from a VAWT tested in an open jet facility were compared against results from the same turbine (and conditions) when the open jet is replaced by a uniform flow.

1.5 Outline of the thesis

The chapter 1 is covered by the introduction. After it, the chapter 2 presents a theoretical background for the aerodynamics involved in VAWTs and the employed ALM for representing it. Validation cases are carried out to compare ALM predictions against experimental measurements, results are presented in chapter 3 along with the discussions related to similarities and discrepancies. This is followed by chapter 4, with the model already validated, where different and diverse study cases with their obtained results are presented. The thesis finishes with the conclusions and suggested future works.

2. Theoretical background

2.1 Aerodynamics of wind turbines

The total available kinetic power from the wind through an area A is expressed as

$$P_{\text{wind}} = \frac{1}{2}\rho A V_\infty^3 \tag{2.1}$$

with ρ as the air density, and V_∞ the velocity of the flow. In case there is no surrounding boundaries to confine the flow, then P_{wind} is the total available kinetic energy available for a wind turbine (which extraction is restricted, among other, by the Betz limit). However, part of the flow interacting with the turbine will change its direction moving outside the rotor area, and hence, the kinetic energy that passes though the cross-section area A. Moreover, the decelerated flow by the turbine still keeps some kinetic energy that can be used later on. Then, the quantification of how good the energy conversion is can be expressed with the power coefficient

$$C_P = \frac{P}{\frac{1}{2}\rho A V_\infty^3}, \tag{2.2}$$

where P is the total power extracted by the turbine and V_∞ the asymptotic flow velocity. This is the most relevant variable in wind turbine aerodynamics. By using this expression, the power extracted by the turbine can be compared against the power that passes through the blade-swept area if the turbine would not be there, instead of comparing against the power that really passes by A. In practice, the power extracted by a wind turbine is expressed in terms of the torque as

$$P = Q\Omega, \tag{2.3}$$

where Q is the turbine torque and Ω is the rotational speed of the rotor. Here, the focus is on lift-based turbines. Therefore, the major contribution for the torque comes from the lift force, and on the contrast, the drag force increases the losses. The normal force F_N can be usually used to express the structural loads on blades since it is the resultant of the aerodynamic forces in the radial component. F_T is directly related to the turbine torque for one revolution as

$$Q = \int_{s_{start}}^{s_{end}} N_B r(s) \langle F_T(s) \rangle ds \tag{2.4}$$

with N_B denoting the number of blades, r the radius of the turbine and $\langle F_T \rangle$ the averaged tangential force within one revolution. When the turbine is supported by struts (e.g. a VAWT with H-rotor), they will also contribute to the

total tangential force (together with the blades). The turbine geometry and operational conditions are the principal parameters for influencing the tangential force.

For an operational turbine, the relative velocity flow V_{rel} (with the spanwise component removed) and the angle of the relative wind φ are obtained through the geometrical relation between the tangential velocity of the blade V_{blade} and the incoming flow V_{in}, which is commonly smaller in magnitude than the asymptotic freestream velocity V_∞,

$$\vec{V}_{\text{rel}} = \vec{V}_{\text{in}} - \vec{V}_{\text{blade}} \tag{2.5}$$

The blade velocity is given as Ωr, where Ω is the angular velocity. Considering a Cartesian coordinate system and assuming that the freestream velocity is aligned in the $x-$axis without any flow expansion ($\vec{V}_\infty = V_\infty \hat{x}$ and $\vec{V}_{\text{in}} = V_{\text{in}} \hat{x}$), the magnitude of the relative flow velocity can be expressed as

$$|\vec{V}_{\text{rel}}| = V_{\text{in}} \sqrt{\left(\frac{\Omega r}{V_{\text{in}}} - \cos\theta\right)^2 + (\sin\theta)^2} \tag{2.6}$$

and the angle of relative wind as

$$\varphi = \arctan\left(\frac{\sin\theta}{\frac{\Omega r}{V_{\text{in}}} - \cos\theta}\right) \tag{2.7}$$

where φ is the sum of the section pitch angle γ and the angle of attack α. An illustration of the velocities and acting forces on the cross-section of the blade for both HAWTs and VAWTs is depicted in figure 2.1. Besides C_P, there is another relevant parameter which is the tip speed ratio (TSR) λ, this dimensionless quantity is defined by the ratio between the blade tip and the asymptotic flow velocities

$$\lambda = \frac{\Omega r}{V_\infty} \tag{2.8}$$

In order to address all above mentioned items to the turbine torque, the expression for the tangential force F_T can be used as

$$F_T = F_L \sin\varphi - F_D \cos\varphi \tag{2.9}$$

where F_L is the lift force which is perpendicular to V_{rel} and the blade span component, while the drag force F_D has the same direction as V_{rel} for both types of turbine.

2.2 The actuator line model (ALM)

The actuator line model (ALM) is a unsteady three-dimensional aerodynamic model used to study the resulting flow around turbines. It is based on the classical blade element model (BEM) theory coupled to a solver for the governing

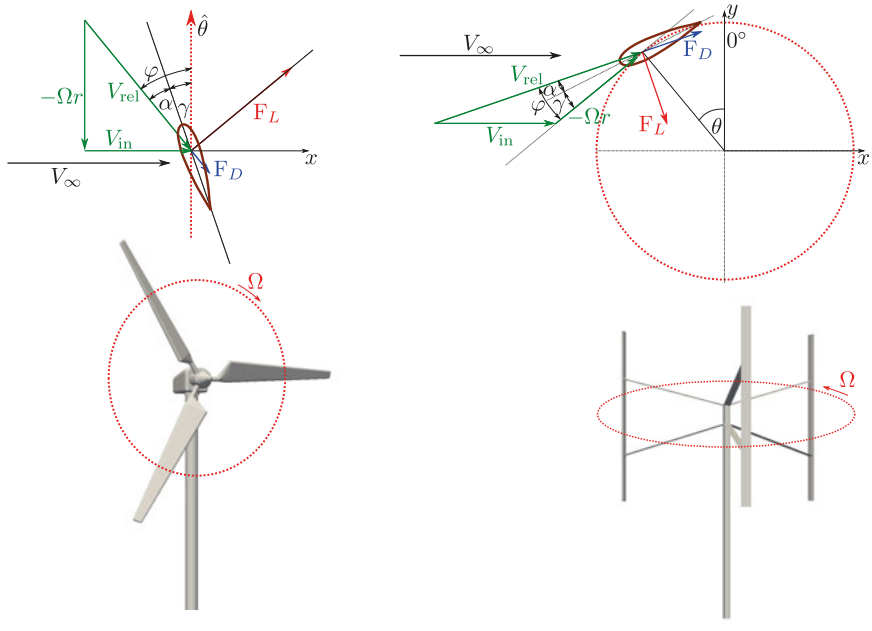

Figure 2.1. Illustration of velocity vectors and forces acting at the cross-section of the blade for a HAWT (left) and a VAWT (right). *Note: For both HAWTs and VAWTs,* $\hat{\theta}$ *denotes the tangential direction of the blade while* θ *is the azimuthal angle for VAWTs.*

Navier-Stokes equations. The ALM, developed by Sørensen and Shen [38], divides the blades in lines of elements which have a two-dimensional airfoil behavior, using given lift and drag coefficients (C_L and C_D, respectively). For VAWTs, the dynamic stall effects on the force coefficient were considered using the Leishman-Beddoes model [39] with the modifications of Sheng [40] et al. and Dyachuk [35]. To do this, the library turbinesFoam developed by Bachant et al. [41–43] was employed to implement the ALM. The original governing Navier-Stokes equations have been considered in their filtered version, using the Large Eddy Simulation (LES) approach for predicting turbulence effects based on an incompressible fluid as

$$\frac{\partial \tilde{u}_i}{\partial x_i} = 0 \tag{2.10}$$

$$\frac{\partial \tilde{u}_i}{\partial t} + \frac{\partial \tilde{u}_i \tilde{u}_j}{\partial x_j} = -\frac{1}{\rho}\frac{\partial \tilde{p}}{\partial x_i} + \nu \frac{\partial^2 \tilde{u}_i}{\partial x_j \partial x_j} - \frac{f_i}{\rho} - \frac{\partial \tau_{ij}}{\partial x_j} \tag{2.11}$$

where $\tilde{u}_i$ and $\tilde{p}$ correspond to the velocity and pressure grid-filtered values, respectively, ν is the kinematic viscosity, f_i the acting body (blade) forces and τ_{ij} is the sub-grid scale (SGS) stress defined as $\tau_{ij} = \widetilde{u_i u_j} - \tilde{u}_i \tilde{u}_j$.

First, the ALM samples the local velocity from the flow solver and then calculates the relative velocity V_{rel} as a vector for each blade element (removing

its spanwise component), from which magnitude and angle can be extracted. Then, the DSM calculates the unsteady lift and drag forces, which the ALM impart back as body forces into the flow solver (figure 2.1). Once α and V_{rel} are calculated, the lift and drag forces per spanwise length unit can be obtained though the expressions

$$f_L = \frac{1}{2}\,\rho\; c\; C_L\,|V_{\text{rel}}|^2 \tag{2.12}$$

and

$$f_D = \frac{1}{2}\,\rho\; c\; C_D\,|V_{\text{rel}}|^2 \tag{2.13}$$

respectively, with c as the chord length and ρ the fluid density.

The implementation of the ALM requires values of C_L and C_D, which are function of the Reynolds number and α. In case the DSM isn't used, these coefficients are obtained through a linear interpolation of a table for a specific α, and using them together with the blade element approach, the body acting forces can be determined. The same procedure is applied for the acting forces on the shaft and struts (for VAWTs). Once all the forces in the lines of elements are calculated, they are added as a source of body force per unit of density into the momentum conservation equation 2.11.

2.2.1 Improved inflow velocity sampling

It is a common practice to consider the inflow velocity which is located at the same place of the element (the quarter chord position). This has been applied in previous studies carried out by Sørensen and Shen for HAWTs [44], Shamsoddin and Porte-Agel for VAWTs [45] and also the US National Renewable Energy Laboratory (NREL) [46], among others. However, in the present work the local velocity is obtained using the averaged value from a defined numbers of local velocity samples which are symmetrically distributed around the quarter chord location. This technique has been implemented in order to reduce the effect of the blade bound circulation affecting the inflow direction and it was developed and implemented by Anders Goude[1]. A study for the sensitivity of this method was carried out showing that 10 to 20 samples at a distance from 2ε to 3ε are appropriated values to consider, where ε is the width of the Gaussian function used in the force projection kernel (equation 2.14).

2.2.2 Calculated force distribution

After the force is calculated with in the element locations it needs to be distributed smoothly on several mesh points in order to avoid numerical instabilities due to high gradients. To overcome this potential issue, the source term of force is projected around the element location from its maximum value using

[1] Senior Lecturer at Dept. of Engineering Sciences, Division of Electricity, Uppsala Univerity

a three-dimensional Gaussian kernel. The employed smoothing function η_F, which is multiplied by the computed local force on the actuator line element and distributed on a cell with a distance $|\vec{d}|$ from the quarter chord location of the actuator line element, is written in the form

$$\eta_F = \frac{1}{\varepsilon^3 \pi^{3/2}} \exp\left[-\left(\frac{|\vec{d}|}{\varepsilon} \right)^2 \right] \tag{2.14}$$

where ε represents the smoothing width parameter of the function, which is chosen by the maximum value from three different contributions related to

- the 25% of the chord length
- the mesh size
- the momentum thickness due to drag forces

and it can be expressed as

$$\varepsilon = \max\left[\frac{c}{4}, 4\sqrt[3]{V_{\text{cell}}}, \frac{cC_D}{2} \right] \tag{2.15}$$

with V_{cell} denoting the volume of the cell, and being $\frac{c}{4} = \varepsilon$ the most case typically used.

2.2.3 Unsteady effects

Within the turbine aerodynamics, particularly in the VAWT type, the ALM faces unsteady conditions in both the angle of attack and the relative velocity. Therefore, unsteady aerodynamic models are needed in order to improve the static airfoil characteristics to capture both the transient response of the attached flow loading and the flow acceleration effects (also known as added mass). Moreover, operating conditions of VAWTs commonly faces high angles of attack, and therefore, dynamic stall phenomena. Then, for an appropriate representation of the blade forces it is needed to model the unsteady detached flow.

Dynamic stall model (DSM)

Dynamic stall appears when the blade quickly changes its angle of attack and exceeds a certain threshold usually close to the static angle of stall [47]. This is characterized by an initial increase in the lift above static values until a vortex is shed from the airfoil leading edge, followed by a lift drop due to the reduced circulation caused by the flow separation.

The employed dynamic stall model (DSM) is based on the one developed by Leishman-Beddoes [39] with the modifications of Sheng et al. [40] and Dyachuk [35]. This model is able to compute the unsteady lift, drag and pitching moment, giving a physical description of the aerodynamics and it has been

Table 2.1. *Empirical constants for the dynamic stall model model*

Airfoil	T_α	$\alpha_{ss}[^\circ]$	$\alpha_{ds0}[^\circ]$	B_1	η	E_0
NACA0012	3.90	14.95	18.73	0.75	1	0.25
NACA0015	5.78	14.67	17.81	0.50	1	0.25
NACA0018	6.22	14.68	17.46	0.50	1	0.20
NACA0021	6.30	14.33	17.91	0.50	0.975	0.15
NACA0025	6.95	13.59	17.22	0.50	0.90	0.18

validated against experimental values in [48]. It consists in three parts (or subsystems): unsteady attached flow, dynamic stall onset and unsteady separated flow part. However, the ALM already handles the unsteady attached flow.

Due to the lag in pressure response, a delayed angle of attack is considered as

$$\alpha_n{}' = \alpha_n - D_{\alpha_n}, \tag{2.16}$$

where D_α as the deficiency function

$$D_{\alpha_n} = D_{\alpha_{n-1}} \exp\left(-\frac{\Delta s}{T_\alpha}\right) + (\alpha_n - \alpha_{n-1}) \exp\left(-\frac{\Delta s}{2T_\alpha}\right) \tag{2.17}$$

with the empirically derived time constant T_α, whose value is in table 2.1, and Δs corresponding to a non-dimensional time-step written as

$$\Delta s = \frac{2|\vec{V}_{rel}|\Delta t}{c}. \tag{2.18}$$

The indices n and $n-1$ denote the current and previous discretized time step. Due to the flow reversal in the boundary layer, a leading edge vortex is created at the airfoil surface. A critical angle of attack α_{cr_n} is considered to define the condition at which dynamic stall starts

$$\alpha_{cr_n} = \begin{cases} \alpha_{ds0} & |q_n| \geq q_0 \\ \alpha_{ss} + (\alpha_{ds0} - \alpha_{ss}) \frac{|q_n|}{q_0} & |q_n| < q_0 \end{cases} \tag{2.19}$$

with the reduced pitching rate q_n defined as

$$q_n = \frac{\dot{\alpha}_n c}{2|\vec{V}_{rel}|}. \tag{2.20}$$

In this expression, $\dot{\alpha}$ represents the pitch rate and q_0 the reduced pitching rate which limits the quasi-steady stall with the dynamic stall and its value is $q_0 = 0.01$ for symmetrical NACA airfoils (see [48]). The static stall onset angle α_{ss} and the critical stall onset angle α_{ds0} values are displayed in table 2.1. The following is the dynamic stall consideration defined as when the delayed angle of attack α' is larger than the critical angle of attack α_{cr}

$$|\alpha'| > \alpha_{cr} \rightarrow \text{stall}. \tag{2.21}$$

The separated flow part include effects that can be divided into two groups: the trailing edge and leading edge vortex separation. The trailing edge separation is related to the temporal delay in the movement of the boundary separation point, and it is calculated using the Kirchhoff's approximation

$$f'_n = \begin{cases} 1 - 0.4\exp\left(\frac{|\alpha'_n| - \alpha_I}{S_1}\right) & |\alpha'_n| < \alpha_I \\ 0.02 + 0.58\exp\left(\frac{\alpha_I - |\alpha'_n|}{S_2}\right) & |\alpha'_n| \geq \alpha_I \end{cases} \tag{2.22}$$

where f' represents the delayed separation point and α_I, S_1 and S_2 are constants, functions of the airfoil profile and the local Reynolds number, which values can be found in [48]. The boundary layer around the blade itself is on function of the time and its effect is superimposed on the pressure response delay (represented by α' in equation 2.16) and it is represented by the dynamic separation point

$$f''_n = f'_n - D_{f_n} \tag{2.23}$$

For this expression, the deficiency function D_{f_n} is

$$D_{f_n} = D_{f_{n-1}} \exp\left(-\frac{\Delta s}{T_f}\right) + (f'_n - f'_{n-1}) \exp\left(-\frac{\Delta s}{2T_f}\right) \tag{2.24}$$

with T_f as an empirically derived time constant from the table 2.1. Therefore, the normal force coefficient for unsteady conditions before the dynamic stall onset is calculated as

$$C^f_{N_n} = C_{N_\alpha} \alpha_n \left(\frac{1 + \sqrt{f''_n}}{2}\right)^2 \tag{2.25}$$

Once the dynamic stall condition is met (equation 2.21), the leading edge vortex convects over the surface of the airfoil towards the trailing edge and then releases. This convection produces a significant increase in the lift forces

$$C^v_{N_n} = B_1(f''_n - f_n)V_x \tag{2.26}$$

where C^v_N represents the normal forces during the vortex convection, which is dependent of the pitch rate. f_n is the static separation point and V_x and B_1 are parameters based on the local Reynolds number and the airfoil profile, they are available in [48]. Once the vortex moves behind the trailing edge, the normal force decreases rapidly. The total normal force obtained is expressed as the sum of the unsteady normal force coefficient and the vortex lift

$$C_{N_n} = C^f_{N_n} + C^v_{N_n} \tag{2.27}$$

Figure 2.2 depicts an example of the normal force coefficient response the during pitching motion of an airfoil using the model described above. The

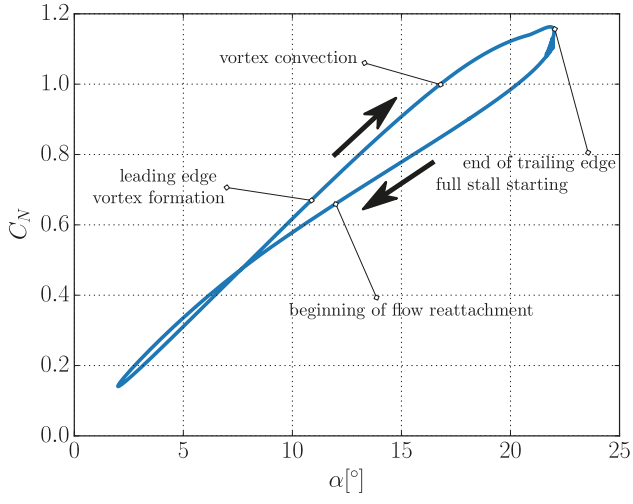

Figure 2.2. Illustration of dynamic stall: NACA0021 profile with $\alpha = 12 + 10\sin(\dot{\alpha}t)$, $\dot{\alpha} = 12.47$[rad/s], $V_\infty = 28.4$[m/s] and c = 0,55[m]

tangential force coefficient C_T, needed to find the lift and drag coefficients, is obtained through the Kirchhoff's flow relation using the dynamic separation point.

$$C_{T_n} = \eta C_{N_\alpha} \alpha_n^2 \left(\sqrt{f_n''} - E_0 \right) \tag{2.28}$$

with the empirical constants η and E_0 which are shown in table 2.1.

Once the normal and the tangential force coefficients are calculated, lift C_L and drag C_D coefficients are obtained as

$$C_{L_n} = C_{N_n} \cos\varphi_n + C_{T_n} \sin\varphi_n \tag{2.29}$$

$$C_{D_n} = C_{N_n} \sin\varphi_n - C_{T_n} \cos\varphi_n + C_{D_0} \tag{2.30}$$

with C_{D_0} denoting the drag coefficient at zero angle of attack, and φ as the relative wind flow angle, which is obtained from the ALM.

Additional corrections must be considered and implemented in the ALM for VAWTs since blade vorticity can be released faster in the downwind side of the rotor due to the circular motion of the blades. Figure 2.3 reveals the vortex shedding structures produced by a Darrieus turbine within a water channel operating at a low TSR $\lambda = 2.14$. This figure is reproduced by the using velocity measurements of the straight-bladed turbine, obtained by Brochier et al. [49]. At quadrant III, both leading and trailing edges vortices are detached and shed, hence, the flow is fully separated and the delay in the separation is absent. For modeling this faster vortex release at the leading and trailing edges, the delay in the angle of attack and the vortex lift values have to be set to zero

$$\text{Quadrant III} \rightarrow \alpha' = \alpha,\ C_N^v = 0 \tag{2.31}$$

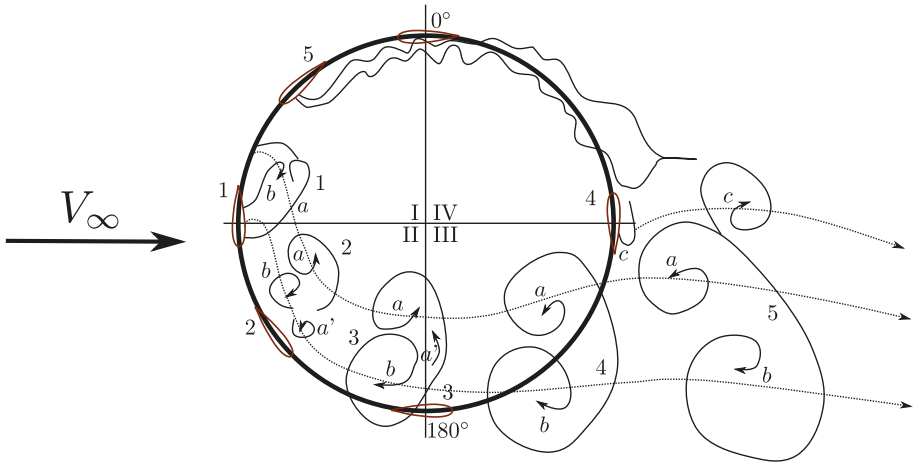

Figure 2.3. Schematic diagram for vortex shedding and dynamic stall condition at $\lambda = 2.14$, taken from Ref. [49]. a, a', b and c denote vortices.

Added mass

The sub-model from Strickland et al. [50] has been implemented for correcting the effects due to the flow acceleration (also known as added mass), which was derived by considering a pitching flat plate in potential flow. In the coordinate system of the blade element the normal and chordwise (in the direction from the trailing to the leading edge) coefficients produced by the added mass are represented as

$$C_{N_{\mathrm{AM}}} = -\frac{\pi c \dot{V}_{\mathrm{rel},N}}{8|V_{\mathrm{rel}}|^2} \tag{2.32}$$

and

$$C_{T_{\mathrm{AM}}} = \frac{\pi c \dot{\alpha} V_{\mathrm{rel},N}}{8|V_{\mathrm{rel}}|^2} \tag{2.33}$$

respectively, with $V_{\mathrm{rel},N}$ as the normal component of the relative velocity, and with the temporal derivative applied in the dotted parameters, which were obtained using a simple first order backward finite discretization. In a similar way, the quarter-chord moment coefficient resulting from the added mass was obtained as

$$C_{m_{\mathrm{AM}}} = -\frac{C_{N_{\mathrm{AM}}}}{4} + \frac{V_{\mathrm{rel},N} V_{\mathrm{rel},T}}{8|V_{\mathrm{rel}}|^2} \tag{2.34}$$

where $V_{\mathrm{rel},T}$ represents the tangential component of the relative velocity. The resulting lift and drag coefficients by the effect of added mass are

$$C_{L_{\mathrm{AM}}} = C_{N_{\mathrm{AM}}} \cos\varphi + C_{T_{\mathrm{AM}}} \sin\varphi \tag{2.35}$$

and

$$C_{D_{\mathrm{AM}}} = C_{N_{\mathrm{AM}}} \sin\varphi - C_{T_{\mathrm{AM}}} \cos\varphi \tag{2.36}$$

respectively. Once the coefficients are already calculated they must to be added to those obtained by the DSM.

2.2.4 Flow curvature correction

The rotating blades of VAWTs have a variable angle of attack due to their circular movement resulting in flow curvature effects [51]. This makes complicated to define a singular angle of attack for interpolation in the force coefficients tables. Moreover, this effects is more relevant in turbines with a high (c/r) ratio. In the present work the flow curvature effects derived by Goude [33] are employed. The corrections consider a flat plate moving through a circular path in potential flow, for which the affective angle φ (contemplating the flow curvature effects) is represented by

$$\varphi = \varphi_{\text{uncorrected}} - \frac{\Omega c}{2V_{\text{rel}}}. \tag{2.37}$$

It should be noticed that for a VAWT, this correction offsets the angle of attack increasing its magnitude on the first half of a revolution and decreasing in the downwind half (due to the negative angle of attack).

2.2.5 End effects

As a consequence to Helmholtz's second vortex theorem, the lift distribution of finite span airfoils must drop to zero at the tips. According to [52], from Pranttl's lifting theory, the geometric angle of attack α can be denoted as a function of the non-dimensional location θ as

$$\alpha(\theta) = \frac{2S}{\pi c(\theta)} \sum_{n=1}^{N} A_n \sin\theta + \sum_{n=1}^{N} nA_n \frac{\sin n\theta}{\sin\theta} + \alpha_{L=0}(\theta) \tag{2.38}$$

with S as the total length of the span, $c(\theta)$ as the chord length as function of the span and N representing the number of elements sampled along the airfoil. This equation can be set into its matrix form in order to solve the unknown Fourier coefficients A_n

$$[\alpha_m] - \alpha_{L=0} = [D_{mn}][A_n] \tag{2.39}$$

where

$$D_{mn} = \left[\frac{2b}{\pi c_m} \sin n\theta_m + n \frac{\sin n\theta_m}{\sin\theta_m} \right]. \tag{2.40}$$

Once the Fourier coefficients are obtained, the circulation distribution can be calculated as

$$\Gamma(\theta) = 2SV_\infty \sum_{n=1}^{N} A_n \sin n\theta \tag{2.41}$$

which through the Kutta-Joukowski theorem gives the correction factor of the distributed lift coefficient

$$C_L(\theta) = \frac{-\Gamma(\theta)}{\frac{1}{2}cV_\infty} \tag{2.42}$$

whose values varies between 0 (at the tips) and 1.

2.3 The recycling method for simulating the atmospheric boundary layer (ABL)

Within the LES framework, it is crucial to properly reproduce the transient inflow conditions for a correct modeling of the ABL interaction with wind turbines. In many previous LES studies dealing with the ABL like [53, 54], a separated LES precursor calculator for ABL flow over a flat terrain has been used to produce the transient inflow boundary conditions. However, the employment of this technique demands a large computational time since it needs the whole simulation to be carried our in two stages: firstly, a precursor simulation of the ABL flow over the whole domain (i.e. without considering the turbine) saving the instantaneous field results in each time step, and then, use the already saved data for the time-dependent main simulation (i.e. ABL with turbine). Moreover, this approach is restricted to simple and generic flows.

In the presented work, the so-called recycling method is employed to produce the fully developed ABL flow profiles before facing the turbine. Chadhauri et al. [55–57] have studied and evaluated the reliability of the recycling method for ABL flow modeling over complex terrains, later on, validating it by the comparison of the obtained results against experimental field measurements. A detailed description of the method can be found in [55–57], and only a brief description is given further in this section.

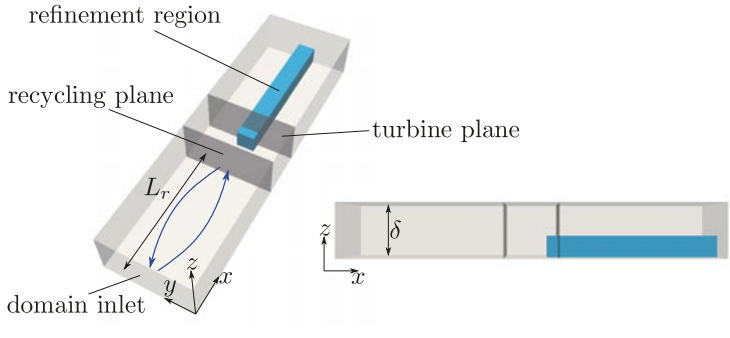

Figure 2.4. Schematic picture explaining the recycling method in a numerical simulation.

By using the recycling method, the precursor and main simulations are combined. During the simulation, the flow variables velocity, SGS turbulent

kinetic energy, etc. are sampled on a perpendicular plane to the main flow (recycling plane) and which downwind distance is large enough from the domain inlet cross-section as it is shown in figure 4.3. Then, the sampled data is recycled back into the inlet plane. This process is repeated for each time-step creating a recycling region between the inflow and the recycling plane, where the flow gradually becomes fully developed. The method is highly sensitive to the length L_r of the recycling zone. After several sensitivity tests, Chadhauri et al. [55–57] suggested that L_r should be at least three times the the ABL depth δ ($L_r \geq 3\delta$), which is considered as $\delta = 5D$ for the tested cases in this thesis. This restriction is required in order to avoid any artificial turbulence structures within the recycling region (due to a short L_r). Additionally to the recycling data, the method employs a fixed flux at the inlet for maintaining the same volume of flow along the entire simulation. The most important advantage of this method is that there is no need of a precursor simulation since the whole simulation is done on a single computational domain as it is displayed in figure 4.3.

2.3.1 Wall-function

Surface boundary condition is another representative challenge for LES simulations. In order to avoid an excessive computational cost solving the boundary layer on surfaces, the use of wall-functions has become somehow a standard procedure nowadays for LES modeling of ABL flows ([55–59]). Furthermore, the surface roughness parameters (height or length) of a rough surface are often implemented via wall-functions. In this work, a log law based wall-function is used on the lower (ground) surface. This wall-function is implemented in OpenFOAM and it was developed by Chaudhari et al. [55, 57, 60]. The logarithmic law over rough surfaces is expressed as

$$V_x = \frac{V_{x*}}{K} ln\left(\frac{z+z_0}{z_0}\right) \tag{2.43}$$

where z_0 corresponds to the ground roughness length, $K = 0.41$ is the von-Kármán constant, and V_{x*} is the instantaneous frictional velocity. The wall shear stress can be denoted using the effective viscosity term $\mu_{\text{eff}} = \mu + \mu_{\text{SGS}}$ such that

$$\tau = (\mu + \mu_{\text{SGS}})\frac{dV_x}{dz} \approx (\mu + \mu_{\text{SGS}})\frac{V_{xp}}{z_p} \tag{2.44}$$

where μ represents the viscosity of the fluid, μ_{SGS} is the sub-grid scale (SGS) viscosity and the subscript p denotes the values of the velocity at the first interior nodes from the wall. By using the definition of the friction velocity $V_{x*} = \sqrt{\tau_w/\rho}$ and the kinematic viscosity $\nu = \mu/\rho$, therefore is obtained

$$V_{x*}^2 = (\nu + \nu_{\text{SGS}})\frac{V_{xp}}{z_p}. \tag{2.45}$$

Consequently, the boundary condition for ν_{SGS} at the wall can be obtained through

$$\nu_{\mathrm{SGS}} = \frac{V_{x*}^2}{V_{xp}/z_p} - \nu, \tag{2.46}$$

where V_{x*} derives from the equation 2.44

$$V_{x*} = \frac{V_{xp}K}{ln(z_p/z_0)}. \tag{2.47}$$

3. Validation cases

In the present section, experimental and numerical results from tested cases with various types of configuration are compared for validating and evaluating the accuracy and reliability of the employed model: a pitching airfoil within a wind tunnel, both horizontal and vertical wind turbines also operating inside a wind tunnel, and additionally, a VAWT which is located at an open site. The performance of the model is tested evaluating the prediction of the acting forces on the blades, the proper representation of the resulting flow field (wake structure) and the estimation of the obtained power.

3.1 Pitching experiments at Glasgow University

A NACA0021 airfoil has been tested at a Reynolds number of around 10^6, which is a reasonable value for operating VAWTs, during a pitching motion similar to the one made by a VAWT blade. Several pitching amplitudes were studied: 13.8°, 17.4° and 22.6° (which correspond to a TSR of λ = 4.19, 3.34, and 2.60 respectively) in order to cover a wide range of operational conditions from shallow to deep stall. When using fixed blades on VAWTs, the angle of attack is a function of the turbine TSR. The variation of the angle of attack that a blade experiences, analog to the airfoil pitching motion, is represented through the function

$$\alpha = \arctan\left(\frac{\sin\theta}{\lambda + \cos\theta}\right) \tag{3.1}$$

where θ is the azimuthal blade angle, λ the TSR and α represents the geometric angle of attack, and it differs from the effective angle of attack α_E, which is used by the DSM for obtaining the proper force coefficients. The NACA0021 profile has a chord length of 0.55 m and it is driven to the dynamic stall regime through the pitching motion described by the equation 3.1. The experimental activity for the pitching blade was carried out at Glasgow University [61].

The reduced frequency k is employed for expressing the blade pitch frequency

$$k = \frac{\omega c}{2V_\infty} \tag{3.2}$$

and for the tested cases it has a value of $k = 0.05$, corresponding to the rotational speed of the turbine equals to $\omega = 5.1$ rad/s.

Numerical results obtained for C_N and C_T are compared against measurements. The studied cases were simulated considering a domain geometry comparable to the wind tunnel used in [61] in order to replicate the pitching blade experiments: a chamber of 1.61 m on the span direction perpendicular to the flow, 2.13 m of height, 2.5 m upwind and 4 m downwind from the blade. A uniform flow of 28.4 m/s at the inlet and a non-slip condition in the walls were defined as velocity boundary conditions. Note that in this study, the flow velocity was sampled at the quarter chord position without considering the improved sampling approach (section 2.2.1).

Normal and tangential force coefficients

For a TSR of $\lambda = 4.19$, both normal and tangential coefficients peak values and curve trends are similar to the experimental data, as is depicted in figure 3.1. There is a slight underestimation of the tangential force coefficients values. In this operating condition the flow is attached since blades are not in the dynamic stall region. Hence, the model has a good performance in the prediction of experiments when using unsteady attached angle of attack calculations.

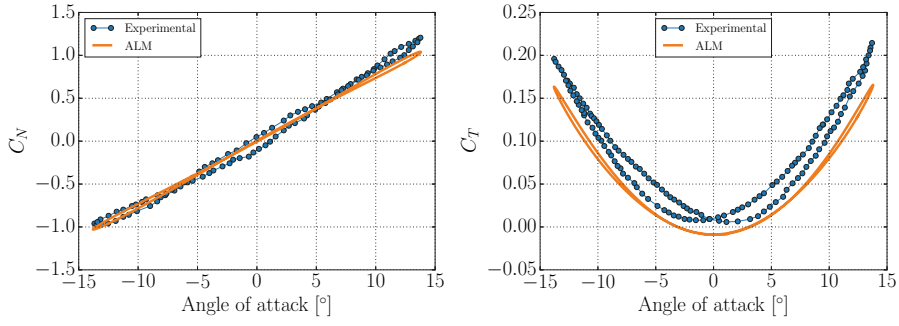

Figure 3.1. Normal (left) and tangential (right) force coefficients during pitching motions of a NACA0021 airfoil with a maximum amplitude of 13.8° (analog to $\lambda = 4.19$).

For the case with a TSR of $\lambda = 3.34$, shown in figure 3.2, the operation regime reaches a maximum magnitude in the angle of attack of $\alpha = 17.5°$, therefore it is in the dynamic stall region. The calculated results for both coefficients show a delay in the reattachment of the flow, which is a characteristic effect of the dynamic stall phenomena. The magnitude of the coefficient peaks are similar between simulated and measured values. Also, there is a good prediction of the stall onset angle flow reattachment.

The case with TSR of $\lambda = 2.60$ is represented by a deep stall condition since the maximum amplitude in the magnitude of attack is $\alpha = 22.6°$, as it is shown in figure 3.3. This is clearly identified by the wider shape of the cyclic force coefficient curves at low TSR operation, and additionally, there is a pronounced delay on the flow reattachment. The C_T peak is overestimated for the positive values of the angle of attack.

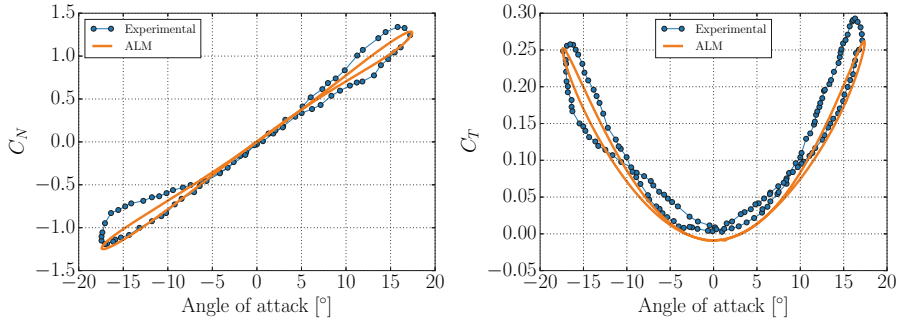

Figure 3.2. Normal (left) and tangential (right) force coefficients during pitching motions of a NACA0021 airfoil with a maximum amplitude of 17.4° (analog to $\lambda = 3.34$).

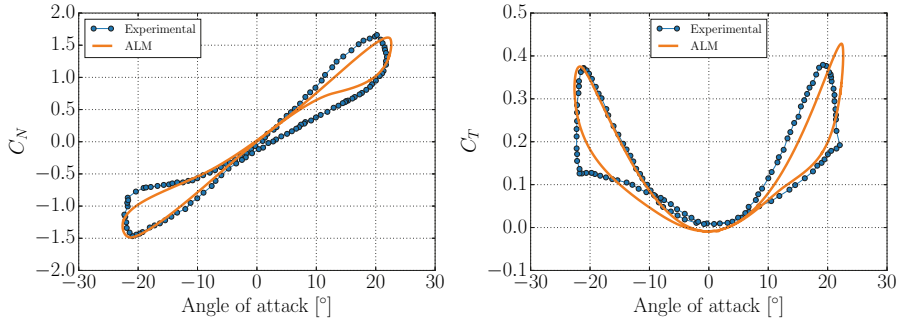

Figure 3.3. Normal (left) and tangential (right) force coefficients during pitching motions of a NACA0021 airfoil with a maximum amplitude of 22.6° (analog to $\lambda = 2.60$).

Discussions

The model was able to properly reproduce the cyclic force coefficient curves for a wide range of TSRs operating conditions, and hence, the different dynamic stall regimes. A good qualitative and quantitative agreement with measurements is emphasized. The trend, magnitude and amplitude of forces are well predicted. Also, it is possible to identify the reattachment point, which is characteristic of the dynamic stall region.

3.2 12 kW Straight-Bladed Vertical Axis Wind Turbine in an open site, Marsta-Sweden

A 12 kW turbine, which is located at an open site was studied. This turbine has a diameter of 6.48 m and it is located North of Uppsala, Sweden. This turbine, shown in figure 3.4, is equiped with four load cells in order to measure the loads on one blade and its struts.

The experimental activity and measurements for the power coefficient curve and the aerodynamic normal forces are available in [14], [28] and [62]. Table

Figure 3.4. The 12 kW turbine, designed and built by the Division of Electricity at Uppsala University. The turbine is equipped with load cells used for the force measurements [14].

Table 3.1. *Specification of the 12 kW VAWT used for validation*

Number of blades	3
Turbine diameter	6.48 m
Hub height	6.0 m
Blade length	5.0 m
Airfoil profile	NACA0021
Chord length	25 cm
Blade pitch angle	2°
Optimal TSR	3.44

3.1 shows relevant specifications of the tested device. The central shaft, blade tapering and struts were considered in the simulations.

The turbine is operating in such conditions that the freestream flow is defined by the log law (equation 2.43). The freestream velocity V_∞ at the equatorial plane $z = 5.75$ m, varies as a function of the tested λ. In the present study z_0 equals to 0.025 m, which corresponds to an open flat terrain and it is an appropriate value for describing the surface roughness of the terrain where the turbine is placed. Numerical results are compared against experimental data, similarities and discrepancies are discussed.

The employed lift and drag coefficients were taken from two different sources: the technical report of Sheldahl and Klimas [63], which is a well known database containing the values for a wide range of Reynolds numbers, and also, from the program for airfoil design XFOIL [64]. This allows to test the sensitivity of the model to the variation of the used force coefficients, and addi-

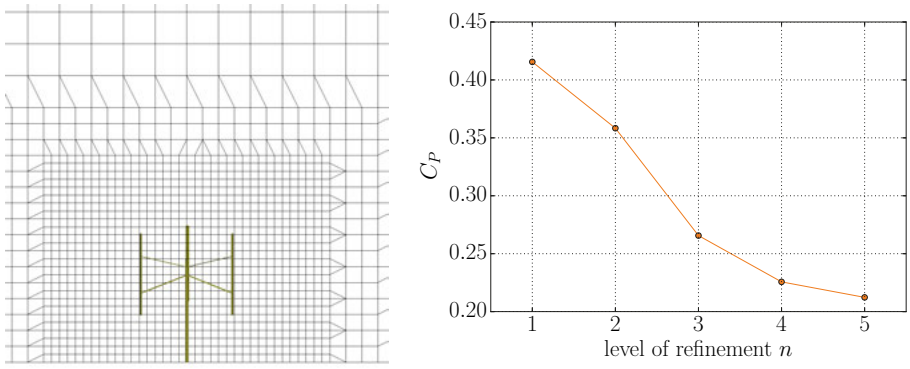

Figure 3.5. Example illustration of the reference mesh section with a local refinement level of $n = 2$ (left) and the power coefficient response for mesh variation using different level of refinement (right).

tionally its influence on the accuracy of the results. These two different ALM versions are further denoted as ALM-SK and ALM-XFOIL, respectively.

Power curve

A reference mesh topology with a hexahedral cells distribution in the whole domain and a cell size of 2 m in every direction has been used for a spatial sensitivity test. For this purpose, a local refinement was applied in the region close to the rotor in order to capture the details of the resulting flow and test the model response to the variation of the mesh discretization. A range of refinement levels from $n = 1$ to 5 (the original cell is divided into 2^{3n} sub-cells) has been tested for a TSR of $\lambda = 4.02$. An illustration of the mesh refinement and the results of the test are depicted in the figure 3.5. It is expected that a refinement level bigger than $n = 5$ will not produce any considerable variation on the obtained C_P value. A modified version of the VAWT mentioned previously has been employed without considering the load cells, resulting in a smaller diameter of the rotor with $D = 6$ m. Moreover, the blade pitch angle was configured to 0° instead of 2°.

Figure 3.6 displays the simulated and experimental power curve for different tested TSRs using the the two different sources for the input values of lift and force coefficient (for the numerical results). For ALM-XFOIL, a good agreement is noticed between experiments and simulations in terms of the curve trend. This allows to identify at least qualitatively the region where the turbine operates maximizing the performance (highest C_P values) which occurs around $\lambda = 3.5$, while the ALM-SK underestimates C_P along several low and medium TSR values. Neither the ALM-SK nor the ALM-XFOIL have good accuracy in predicting the turbine performance at the larger TSRs.

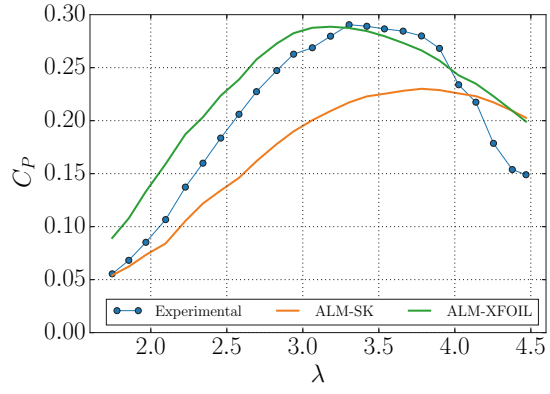

Figure 3.6. C_P as a function of λ.

Normal forces

Numerical and experimental results of normal forces on one blade during one revolution for different TSR are presented in figure 3.7. These results have been studied in a wide range of TSRs with $\lambda = 1.84, 2.55, 3.06, 3.44, 4.09$ and 4.57, and hence, different operating conditions covering from deep until shallow stall. Every experimental result is presented together with the maximum error of measurement. These results correspond to the averaged values of at least five turbine revolutions.

For the cases at low TSRs, with $\lambda = 1.84$ and 2.55, there is an evident overestimation of the force peak in the first half of the revolution (between 0° and 90°). Since these TSRs are characterized by a deep stall, improvements in the DSM are needed for a correct force prediction which is fundamental for the accuracy of the results. Generally there is good agreement in representation of the curve trend and force amplitude (difference between maximum and minimum values). There is a tendency of the model for capturing the experimental force drop close to 270°.

For $\lambda = 3.06$, there is a similar behavior in the results as for $\lambda = 1.84$ and 2.55, although an improvement in the force peak prediction is noticed on the upwind side. Regarding the downwind side, there is no a proper representation of the curve shape by the numerical results, but nevertheless there is a good agreement in the quantification of the force peak value.

It must be considered that inaccurate results on the upwind side directly affect the precision of the results on the downwind side. This is clearly noticed for the study case with $\lambda = 3.44$, where the model showed the best performance. Particularly for this case, the simulated values are reasonably close to the experimental ones for both upwind and downwind sides. Once again, the model is not able to represent properly the force drop in the region around 270°, which is also present for higher TSRs.

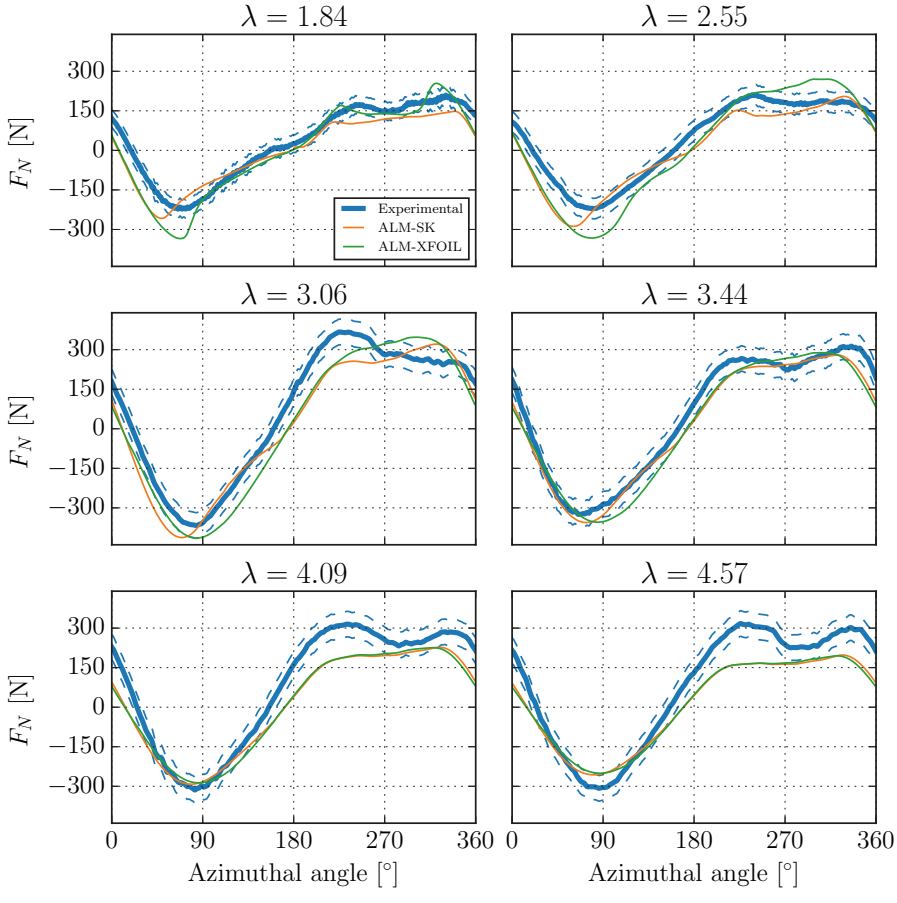

Figure 3.7. The normal force response for one revolution at different TSRs.

For the cases with the higher TSRs, $\lambda = 4.09$ and 4.57, the numerical results are characterized by a good agreement with the experimental normal forces on the upwind side while in the downwind region there is an underestimation of the force drop, which in this case is strongly pronounced. A noticeable smaller force magnitude is predicted by the ALM at $\lambda = 4.57$. In these studied cases with higher TSRs the model was not as accurate as in the previous cases. Both, ALM-SK and ALM-XFOIL models, perform similarly with no relevant differences in the predicted forces.

Influence of the ABL

In the previous studies, the VAWT was tested using a logarithmic velocity wind shear as inflow condition with the results showing a good agreement between numerical and experimental values. An additional test was made for the VAWT operating at its optimal TSR $\lambda = 3.5$ and within an atmospheric

boundary layer ABL which has a surface roughness length of $z_0 = 0.025$m, corresponding to the location where the turbine is installed. The instantaneous streamwise velocity field at the vertical middle plane for both ABL and wind shear has been displayed in figure 3.8. The difference in flow turbulence is easily noticed for both cases, in ABL this is present in the whole domain, while for the wind shear, it appears in the main flow only as a contribution from the turbine blade tips and motion. This effect has been previously studied in detail by Mendoza et al. in [65] obtaining similar results. Also, it is observed that the wake breaks much earlier, as is expected, within the ABL.

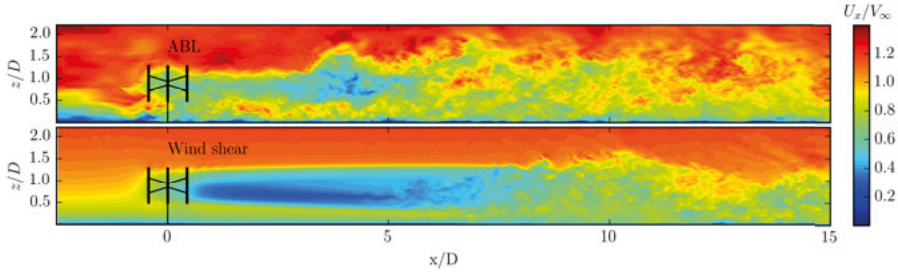

Figure 3.8. Normalized instantaneous streamwise velocity at the vertical middle plane: ABL (top) and wind shear (bottom).

Figure 3.9 depicts the normal force response over one revolution under the influence of both inflows. Numerical results show coherence with experiments in terms of the trend and magnitude. For the case with the ABL, the force peak is overestimated in the first half of the revolution. The results for both inflows are similar in general, and, there is a considerable improvement in the representation of the normal force drop close to 270°.

Discussions

During the numerical work carried out, the ALM-SK revealed an overestimation in the values of the drag forces (drag coefficients) by the employed DSM, resulting in a reduction of the calculated tangential forces, and therefore, on the predicted C_P values. These reduced values of the tangential forces give as compensation a slight increase of the normal forces, which does not influence considerably the obtained flow since its main contribution comes from the lift forces. However, there are improvements required to the DSM for the correct prediction of the drag coefficient C_D, when it is used together with the ALM.

Generally the ALM predicts the upwind side better in all the tested cases. This is expected since during the first half of the revolution the blades face directly the incoming flow, while on the downwind side the blades are operating within the wake, hence, the accuracy on the results for the second half are highly dependent of the proper prediction of the blade forces upwind and the flow field within the rotor.

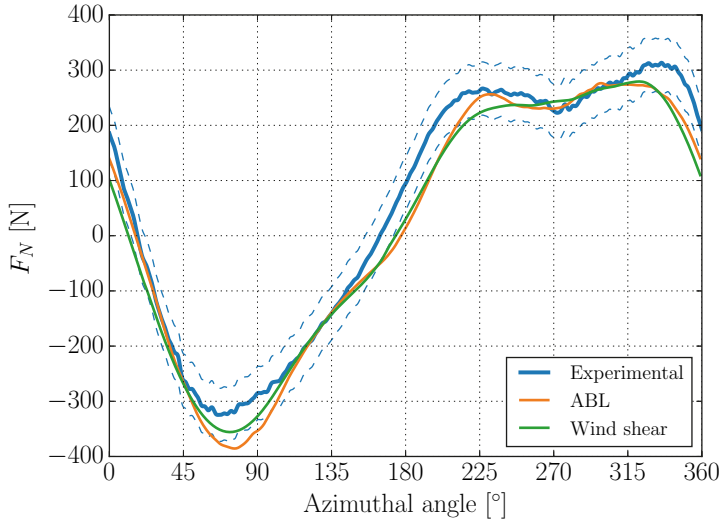

Figure 3.9. The normal force response under the influence of the ABL and a wind shear.

Experimental results at high TSRs show a pronounced force drop on the downwind side, which can be eventually produced by the atmospheric turbulence, since there is a lack of agreement for describing the mentioned phenomenon in the cases with a velocity wind shear at the inlet. However, complementary studies are required in order to check this.

3.3 NTNU two in-line turbines with spanwise offset

This section presents a study based on the experimental activity reported by Krogstad et al. in [66], which has been carried out at the Norwegian University of Science and Technology (NTNU) wind tunnel in Trondheim (Norway), and it consists of two in-line HAWTs which are separated a distance $3D$ in the streamwise direction and $0.415D$ in the spanwise direction. The downwind turbine has a rotor diameter $D_2 = 0.894$ m ($D_2 = D$ is denoted in this section) and a stepped tower consisting of four cylinders of different diameters while the upwind turbine has a slightly larger rotor diameter of $D_1 = 0.944$ m and a tower with constant diameter. This configuration is such that the projection of the upwind rotor area covers the half of the downwind one. The streamwise velocity component has been measured in horizontal (spanwise) lines located $1D$ and $3D$ behind the downwind turbine at the hub height. Experimental data of these velocity profiles and power coefficients C_P of both turbines were compared against numerical values. Figures 3.10 and 3.11 illustrate the mentioned experiment model and schematic views of it.

Figure 3.10. Model in the wind tunnel [67]: perspective (left) and from downwind (right) views

Two different levels of turbulence were tested. Firstly, when the wind tunnel is empty the turbulence intensity level measured at the location of the upwind turbine hub is $T_I = 0.23\%$, this is the so-called case A. Later, a large mesh was installed at the entrance of the chamber in order to reproduce the atmospheric turbulence resulting in a higher measured level of intensity with $T_I = 10\%$, this is denoted as the case B. The synthetic turbulence generator *turbulentInlet* from the standard library of OpenFOAM is used to introduce the different levels of turbulence into the domain. The lift and drag coefficients employed in the ALM were obtained from the work of Cakmakcioglu et al. [68] which correspond to a Reynolds number equivalent to $Re = 10^5$. The upwind and downwind turbines are further denoted as T_1 and T_2, respectively. The domain has been discretized using an mesh with a uniform hexahedral distribution of cells in every directions with a resolution of $16/D$ cells over the whole domain and a locally refined region with $68/D$ cells around and behind the rotor for capturing the details of the resulting flow field.

Power curve

The power coefficients of both turbines were evaluated over a wide range of TSRs. For the studied cases of the downwind turbine performance, the upwind turbine kept operating at its optimal design TSR $\lambda_1 = 6$, where Ω_1 represents the rotational speed of the upwind rotor. The reference freestream velocity is $V_\infty = 10$ m/s and the power and thrust coefficients of the turbines are represented respectively as

$$C_P = \frac{P}{\frac{1}{2}A\rho V_\infty^3} \tag{3.3}$$

and

$$C_{\text{Thrust}} = \frac{T}{\frac{1}{2}A\rho V_\infty^3} \tag{3.4}$$

with P denoting the extracted power and T the thrust of the turbine rotor. Experimental and numerical results are displayed in figure 3.12.

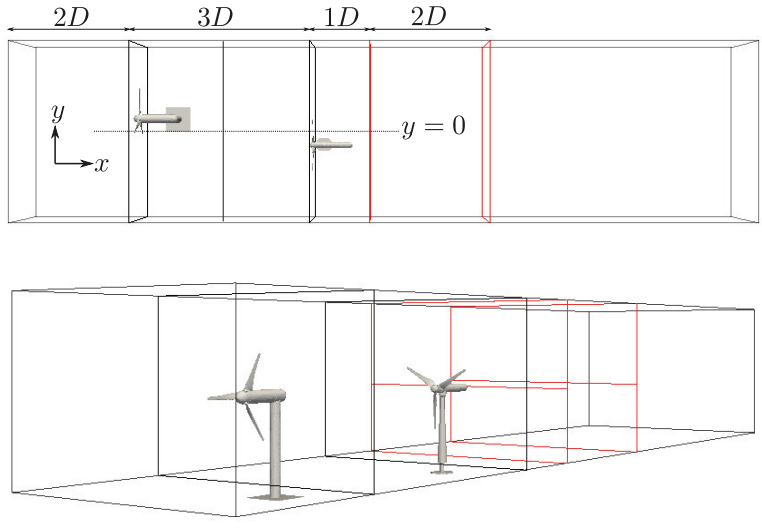

Figure 3.11. Schematic view of the wind tunnel domain: from the upper part (top) and perspective (bottom). The first two perpendicular sections (in black) represent the rotor planes of the turbines, while the two sections after the turbines (in red) represent the plane where the measurements were done, specifically in a spanwise line at the rotor height.

Regarding to the C_P curves representation for the case A, with low turbulence levels in the flow, it can be observed that the model is able to identify the regions where the turbines reach their peak operational performance (optimal λ), and generally, there is a good agreement in the trend of the curves. At the region $\lambda_1 \geq 5$, the accuracy of the model must be highlighted in the prediction of the coefficients for the upwind turbine, contrary to what happens at lower TSRs, where there are notable discrepancies in the stall regime. On the other hand, for the downwind turbine curve, there is a good concordance between simulated and measured values at low TSRs, while an over estimation on the C_P values is present for the cases at $\lambda_2 > 4$. The wake interaction is also captured since for both numerical and experimental results, the values of the C_P curve are lower for T_2 than for T_1 which represents the extraction of kinetic energy by the upwind turbine. For the obtained thrust coefficients, results show that C_T values increase with the increasing of the TSRs. Experimental data of C_T values is similar for both turbines which reveals that almost the same physical forces are applied on the rotors but not the same kinetic energy is available for both. The upwind turbine curve shows a remarkable agreement with simulated results while the numerical thrust coefficient curve of the downwind turbine shows an underestimation over the whole range of tested TSRs.

On the other hand, for the test case B with high levels of flow turbulence, again the model is able to identify the optimal operating region of the turbines.

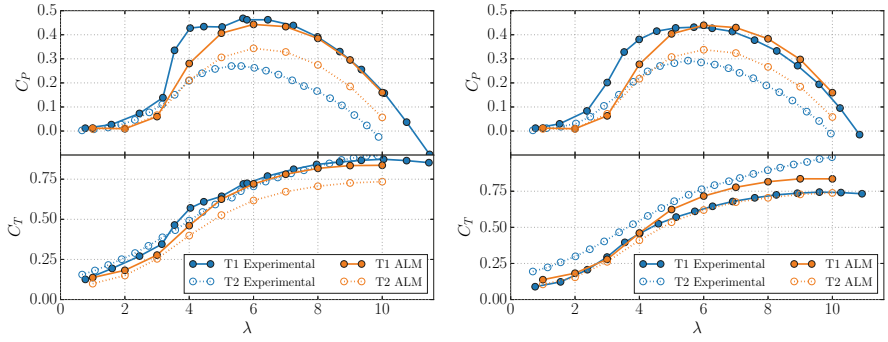

Figure 3.12. Power coefficient and thrust coefficient for the case A with low turbulence level (left) and the case B with high turbulence level (right)

A good numerical representation of the C_P curve happens at $\lambda_1 > 4$ and $\lambda_2 \leq 5$ for T_1 and T_2, respectively. Respecting to the thrust coefficients, numerical values of the upwind turbine are overestimated at $\lambda_1 > 4$, and for the downwind turbine, an underestimation occurs over all the studied TSRs.

Wake: velocity field

The downwind turbine was tested using three different TSRs in order to study the variation on the resulting interacting wakes: for partial stall, optimal TSR and high TSR at $\lambda_2 = 3.5, 4.75$ and 8.0, respectively. Under these conditions the downwind rotor operates from the stall regime until it almost works as a propeller. Numerical and measured values were compared in a horizontal spanwise line at the hub height and a distance of $1D$ and $3D$ behind the downwind rotor. It allows to identify the main structure (flow pattern) of the interacting wake. These results of the velocity deficit profiles were normalized using the freestream velocity V_∞ and are depicted for all the tested TSRs in figure 3.13.

At the location $x/D = 1$ behind T_2, both cases A and B agree in the representation of the wake's general geometry and size as well as in the asymmetric behavior. Small discrepancies can be found on the velocity profile details. Three different regions are recognized: at $-1.5 < y < -0.5$ where the velocity deficit is mainly produced by the upwind turbine T_1, the region for $-0.5 < y < 0.5$ with a resulting wake from both turbines and $0.5 < y < 1.5$ where only the effects of T_2 are present. There is a particular situation for $\lambda_2 = 8.0$ since the blades produces a high flow blockage at the tips and a relatively low one at the roots location. For the section at $x/D = 3$, one can observe a relevant change on the velocity deficit profiles from a irregular shape (at $x/D = 1$) to a smoothly one with a Gaussian distribution of the wake, revealing that at this location the wake recovery process already started, and therefore, the direct contribution from the rotors into the flow patter are dissipated by the turbulent

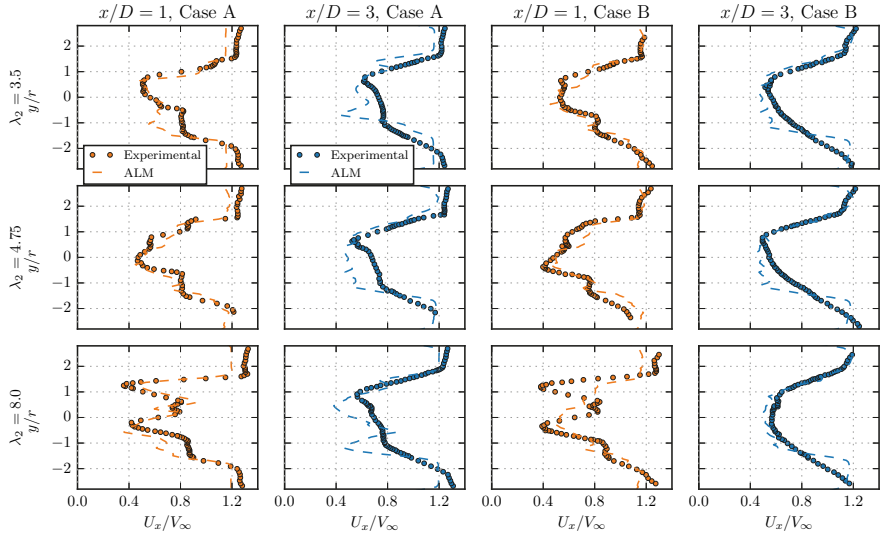

Figure 3.13. Normalized mean streamwise velocity profiles along a spanwise (horizontal) line through the rotor center

structures. Also, a good agreement of numerical and measured values in the region outside from the wake should be highlighted.

The effects produced by the added turbulence in case B are not considerable in the near wake section ($x/D = 1$) where the main structure is dominated directly by the flow-rotor interaction, moreover, at this section for both cases A and B the velocity profiles don't differ relevantly. Differences between the profiles are more pronounced in the far wake section.

Discussions

The author presumes that discrepancies between numerical and experimental results can be mainly due to:

- The employed turbulence generator is not realistic, it is based on the addition of random noise into the velocity field at the inlet from a defined turbulence level since the present work is aiming to validate the model through the velocity flow field prediction.
- The input data used for C_L and C_D are taken from experiments considering only a Reynolds number of $Re = 10^5$. A wider range of data is needed in order to improve the accuracy of the results since the studied cases covers different operational conditions of the turbines and the ALM is highly sensitive to the input data for an appropriate force projection.
- Potential improvements can be achieved in the wake outer regions by fully-solving the wall boundary layers which is not the case in the present study (wall functions were applied).

3.4 Delft TU Open Jet Facility case

An H-shaped VAWT has been tested, which experimental activity was performed for in the Open Jet Facility (OJF) of the Delft University of Technology, and it is documented in [69]. The turbine has two rotor blades projected from a NACA0018 aluminium airfoil profile with a height of $H = 1$ m and a chord length of $c = 0.06$ m. The turbine is operating within a freestream flow with a velocity of $V_\infty = 9.3$ m/s provided by an octagonal jet with a cross-section of $2.85D \times 2.85D$ and a contraction ratio of 3:1 as it is shown in figure 3.14. The rotor has a constant rotational speed of $\omega = 800$ rpm with a radius of $r = 0.5$ m from the symmetry axis, operating with a local Reynolds number of around 2×10^5. The blade chord attachment is located at a distance of $0.4c$ from the leading edge. The tower and the blades are connected through two struts with the NACA0018 profile and with a chord of 0.023 m, which are installed at a distance of 0.2 m from the blade tips.

In order to facilitate the representation of the results, a Cartesian coordinate system has been established with the origin at the point where the equatorial blade plane coincides with the symmetry axis, such that the positive component of the x-axis is pointing in the downwind direction. The positive angular rotation is defined as counter clockwise direction seen from the top of the turbine. Figure 3.14 shows the tested turbine and the schematic of the blades motion.

Velocity and vorticity fields at representative sections of the wind tunnel are analyzed, this will allow the study of the evolution and most relevant phenomena on the resulting wake behind the turbine.

Figure 3.15 depicts the instantaneous streamwise velocity component in the horizontal and vertical middle planes in a large section of the whole domain. The jet flow and expansion are clearly identified as well as the blockage produced by the turbine. A vertical shrinking and an horizontal extension are characteristic of the geometrical wake structure as the flow moves downwind. The region where the wake breaks and the flow recovery process starts is also recognized, the dimensions of the chamber are not large enough to produce a full wake recovery. As it can be expected, stagnation (recirculation) areas are located around the jet.

Spatial and temporal sensitivity

Studies of the sensitivity of the model to the variation of the mesh and temporal discretization were performed. For the mesh variation response, different domain discretizations have been tested using a local refinement resolution of $D/40, D/80, D/96$ and $D/112$ cells in every direction. All the employed domains have the same topology: an hexahedral distribution of cells with a local refinement in the region within and around the turbine rotor. This topology was kept constant and globally refined (mesh proportionally scaled) in every coordinate.

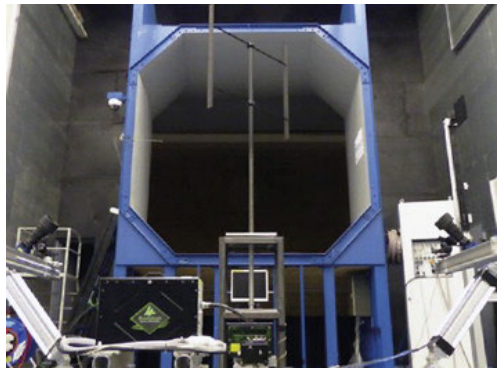

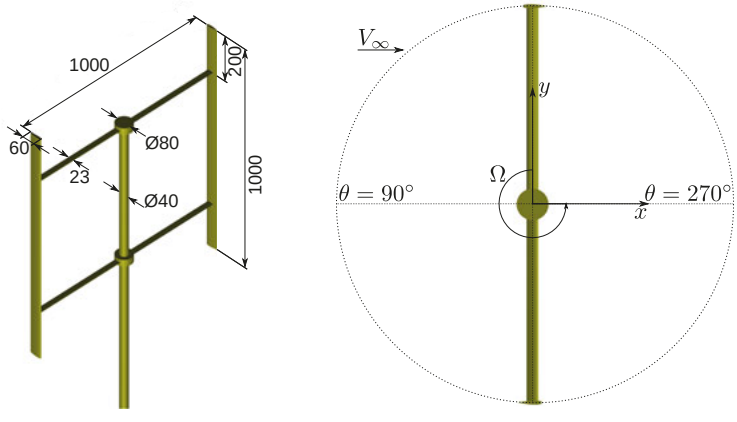

Figure 3.14. OJF tested turbine in [69] (top), 3D drawing of the simulated VAWT for this study with dimensions in [mm] (left) and schematic of the blade motion (right).

Figure 3.16 shows the obtained streamwise velocity component varying the discretization of the domain. It can be observed that the results have good agreement with the experimental data for all the mesh configurations, and moreover, there is not a considerable improvement on the accuracy when increasing of the mesh resolution in terms of average values. However, the highly refined meshes result in curves with more irregular shape since the model is able to capture more details from the wake.

To verify the temporal sensitivity, different maximum Courant number values have been chosen in a test for the response to the variation in the time discretization: 0.25, 0.5 and 0.95. The results were obtained using the mesh with $D/80$ cells of resolution and they are shown in figure 3.17. Numerical streamwise velocity profiles have good agreement with experiments. Comparing these results with the ones achieved in the spatial sensitivity test (figure 3.16), it is observed that the model is much more sensitive to varying the mesh resolution than to the temporal discretization. Previous work carried out by Bachant et al. [70] and Mendoza et al. [71] showed the same attribute.

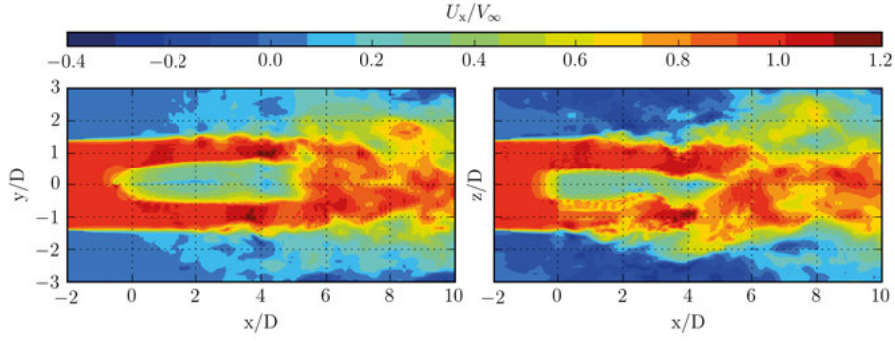

Figure 3.15. Instantaneous normalized streamwise velocity in the horizontal (left) and vertical (right) middle planes.

Horizontal plane

Horizontal planes of streamwise velocity, cross-stream velocity and out-of-plane vorticity are depicted in figures 3.18, 3.19 and 3.20, respectively. Experimental result plots are located on the left side of the figures, while the numerical ones at the right side. Values have been normalized using the asymptotic velocity and the chord length for simplifying the analysis and comparison. The lateral structure of the wake is identified and, therefore, the contribution from the blade pitch motion on it.

Overall, there is a good agreement in the wake representation in the whole studied region, including within the rotor ($-0.5 \leq$ x/D ≤ 0.5). A pronounced secondary wake is produced by the rotating shaft of the turbine, which has a slight inclination towards the positive $y-$direction. The general structure of the wake has a lateral expansion in the $y-$direction and the simulated results underestimate it, as well as the region of higher wake deficit ($U_x/V_\infty \sim 0.2$). Accelerated flow ($U_x/V_\infty \sim 1.1$) is present downwind of the rotor, in the outer region of the wake. The vortical structures created by the motion of blades are dissipated along the main flow direction. These structures are well represented after the rotor with a better accuracy on the negative $y-$direction. Experimental and simulated results show smooth effects since they were obtained from an averaging process [69]. There is a good simulated representation of the blades interaction with the inner rotor wake.

Vertical planes

Figures 3.21, 3.22 and 3.23 show the streamwise, cross-stream and vertical velocity components, respectively, at different representative vertical planes sections: $y/D = -0.5, -0.4, -0.2, 0, 0.2, 0.4$ and 0.5. This allows to represent and identify the vertical shape, extension and location of the wake, and additionally, how this is affected by the vorticity released by the blade tips. As it was done previously, with the horizontal plane study, the results have been normalized using the asymptotic velocity and length of the chord.

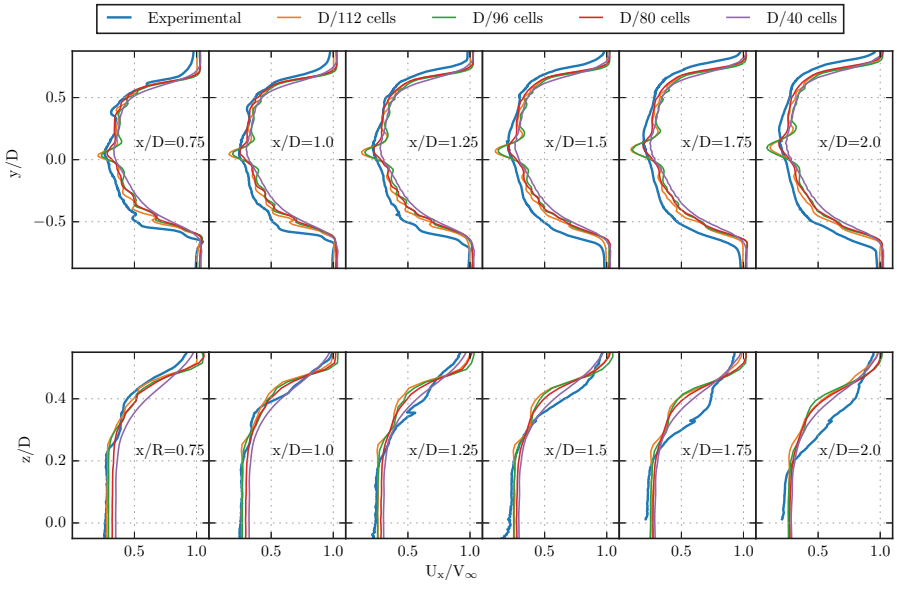

Figure 3.16. Comparison of the spanwise (top) and vertical (bottom) profiles of the normalized mean streamwise velocity at different downstream sections x/D, for domain meshes with $D/40, D/80, D/96$ and $D/112$ cells.

A good agreement is obtained by the numerical results in all sections, however, a better performance is present in the regions close to the rotor with a loss of concordance on further downwind distances. Vortical structures from the blade tips are well represented, specially in the section close to the middle vertical plane (y $\sim$ 0). One can notice the dissipation of the vortices along the main flow direction in figure 3.23. Even though their position is properly simulated, the size is underestimated. This same happened in the horizontal plane, resulting in a smaller wake expansion in both vertical and horizontal directions for the numerical results. Hence, the simulated wake is characterized by a lower wake deficit. Contribution from the tower is evident on the vertical middle plane ($y/D = 0$) where this obstructs the flow.

Figures 3.22 and 3.23 reveal the inner wake characteristics. The cross-stream flow field shows the lateral expansion of the wake and its components are pointing outwards the middle plane section.

Discussions

The ALM as a simplified model can generate a proper representation of the general structure of the wake, but there is a an underestimation on the vorticity created by the blade tips and struts resulting in a less accurate vertical expansion of the wake. This could be produced by force prediction issues since the model showed a high sensitivity for it.

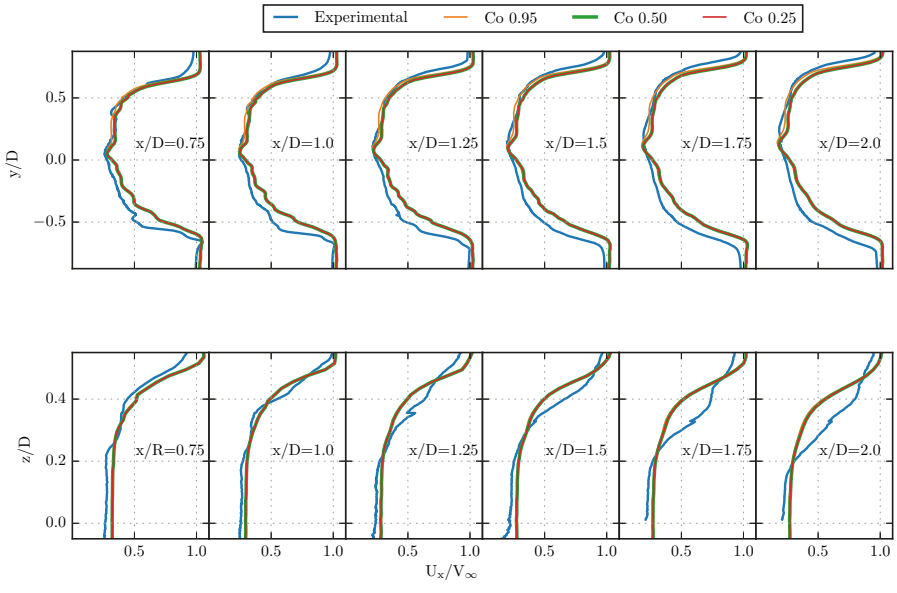

Figure 3.17. Comparison of the spanwise (top) and vertical (bottom) profiles of the normalized mean streamwise velocity at different downstream sections x/D, for maximum Courant numbers equal to 0.25, 0.5 and 0.95.

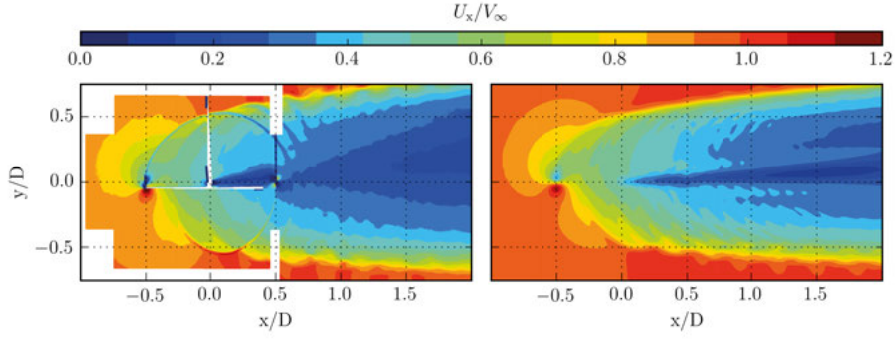

Figure 3.18. Normalized streamwise velocity in the horizontal middle plane for experimental (left) and numerical (right) results.

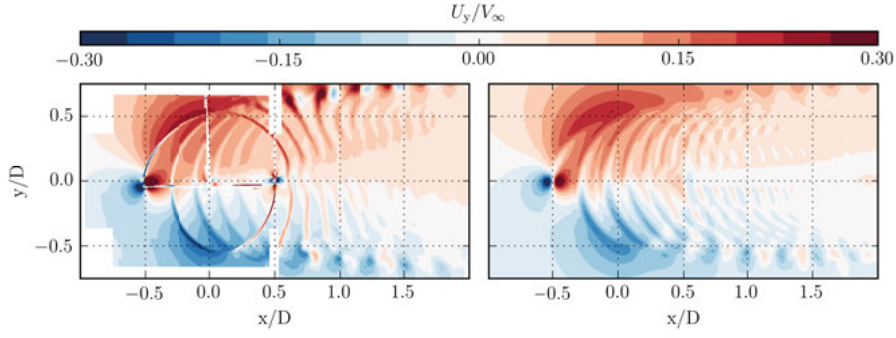

Figure 3.19. Normalized cross-stream velocity in the horizontal middle plane for experimental (left) and numerical (right) results.

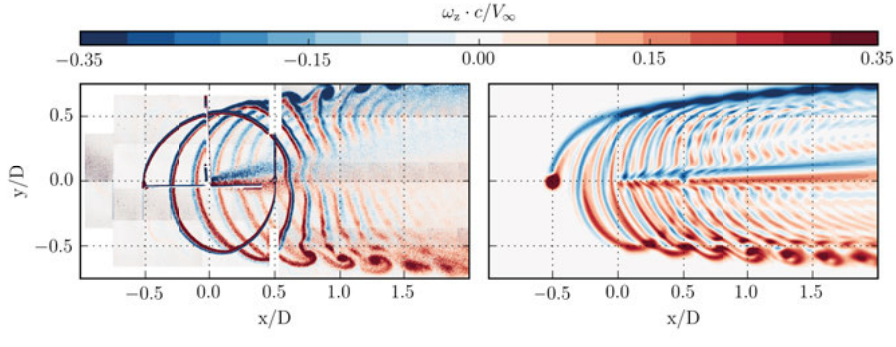

Figure 3.20. Normalized out-of-plane vorticity in the horizontal middle plane for experimental (left) and numerical (right) results.

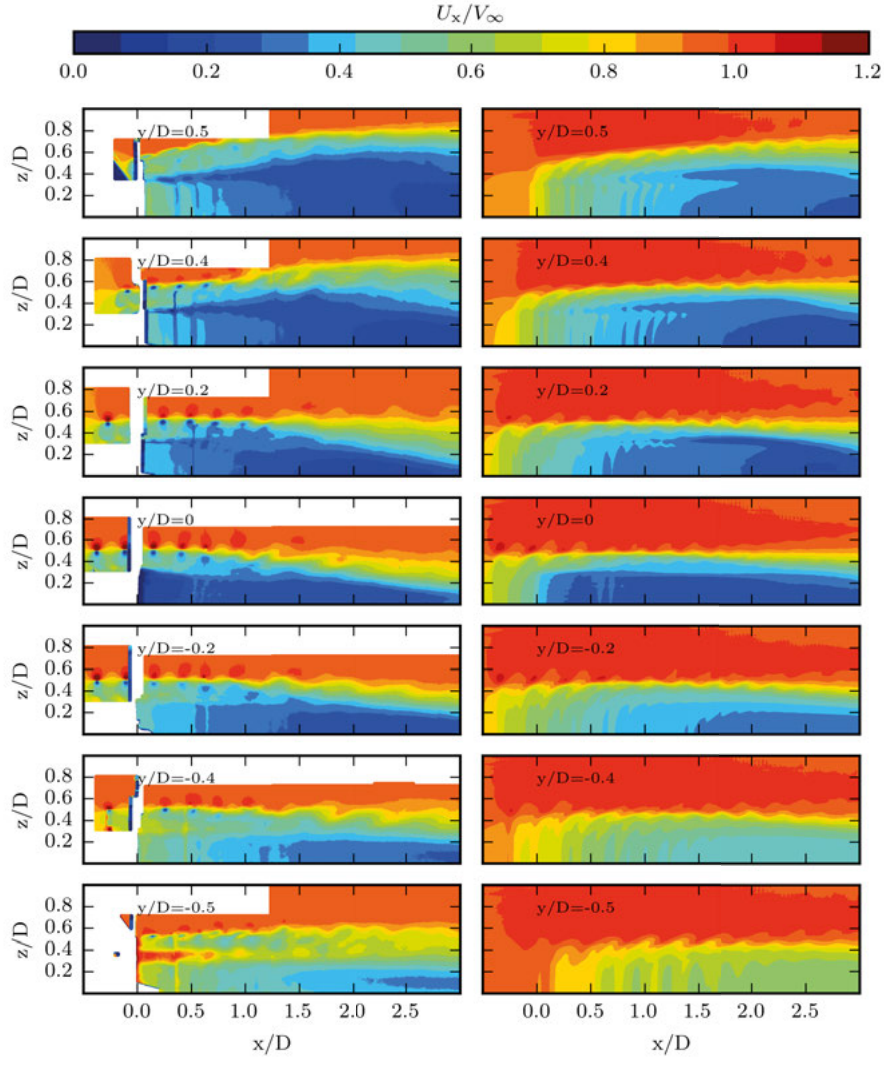

Figure 3.21. Normalized streamwise velocity at different representative sections in the vertical plane for experimental (left) and numerical (right) results.

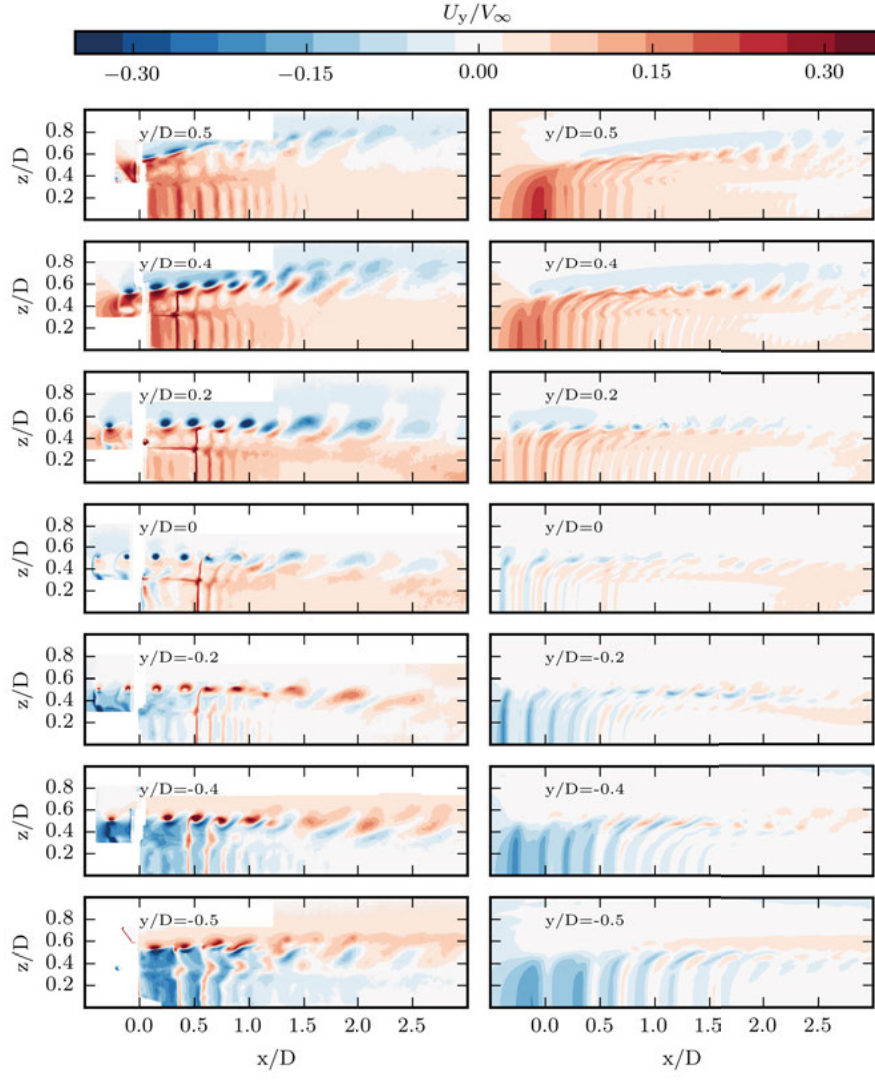

Figure 3.22. Normalized cross-stream velocity at different representative sections in the vertical plane for experimental (left) and numerical (right) results.

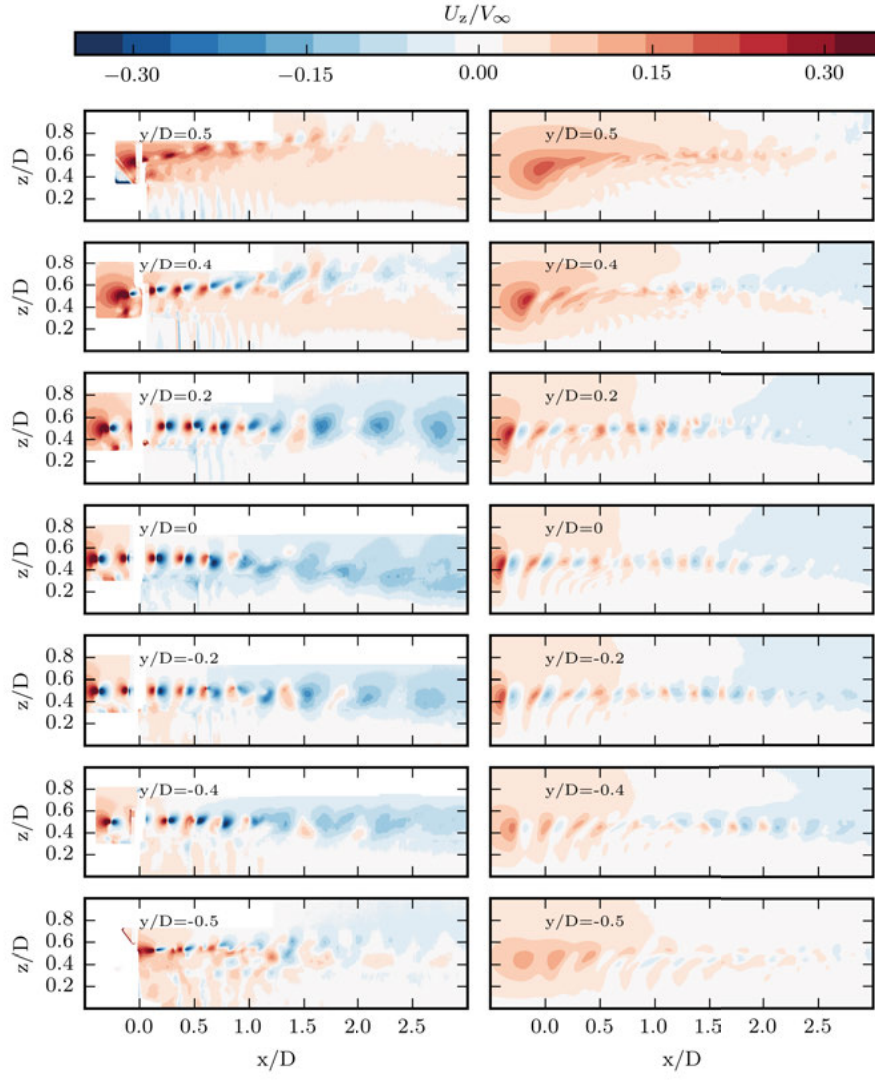

Figure 3.23. Normalized vertical velocity at different representative sections in the vertical plane for experimental (left) and numerical (right) results.

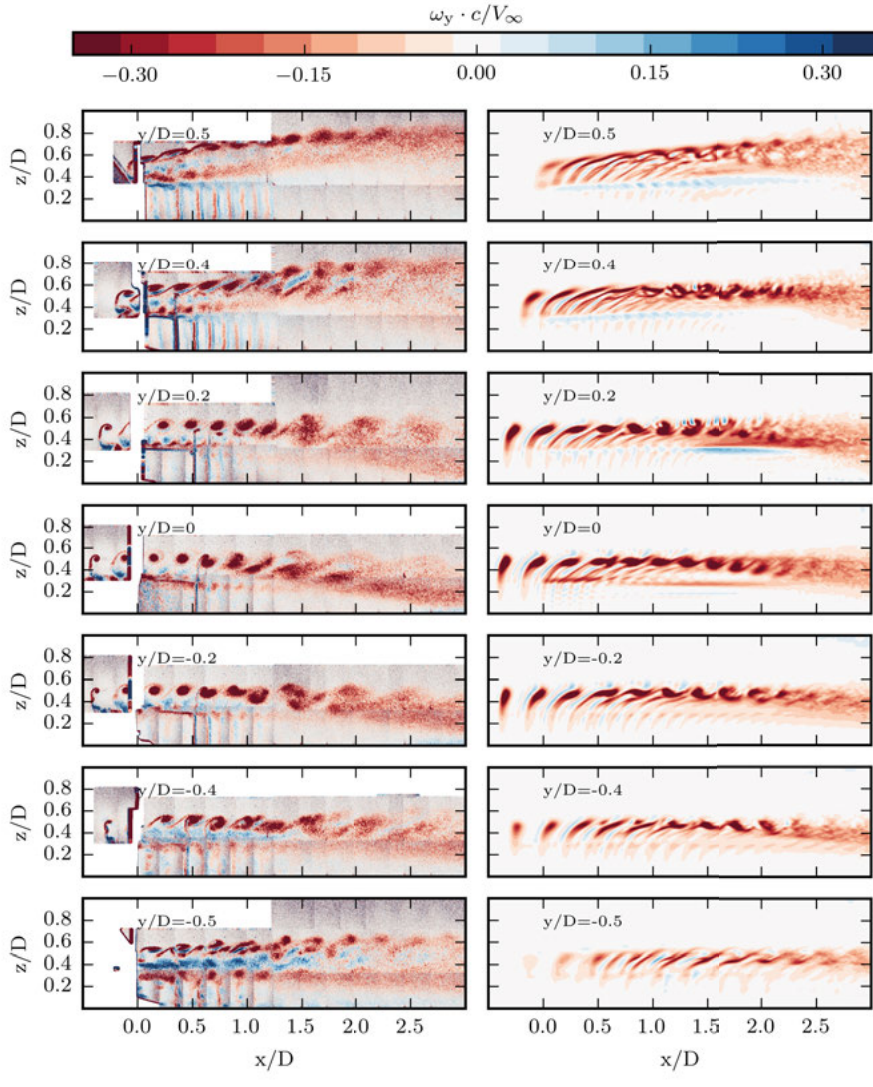

Figure 3.24. Normalized cross-stream vorticity at different representative sections in the vertical plane for experimental (left) and numerical (right) results.

4. Study case results and discussions

This chapter presents the results from numerical studies that have been carried out with the validated ALM.

4.1 Performance and Wake Comparison of Horizontal and Vertical Axis Wind Turbines Under the Influence of the Atmospheric Boundary Layer

A study of the effects produced by the ABL flow on stand-alone wind turbines has been carried out. Both a HAWT and a VAWT within a neutrally-stratified ABL were tested varying the surface roughness length of the terrain. This work aims to evaluate the performance of large scale wind turbines operating at their optimal TSR and how it is influenced by the variation of the atmospheric turbulence, and additionally, to reproduce the main phenomena involved on the resulting wake identifying the general structure of the wake. For every case, both turbines have the same inflow conditions in order to make a fair comparison of similarities and differences in the obtained performance and flow pattern. For this purpose, the well documented NREL 5-MW turbine [72], and an H-type VAWT scaled turbine are studied, the latter turbine is a modified and proportionally scaled version of the VAWT used in the section 3.2 in order to have a similar power rating. The VAWT has the diameter $D = 126$ m which is equal to the blade length H. A standard NACA0021 airfoil with a chord length of $c = 5.25$ m has been used for the cross-section of the blades which have been tapered a distance of 25 m from the tips, where the chord length is 3.15 m. The hub height of both turbines is established at $z_{\text{hub}} = 90$ m as is shown in figure 4.1. Both turbines were tested over a

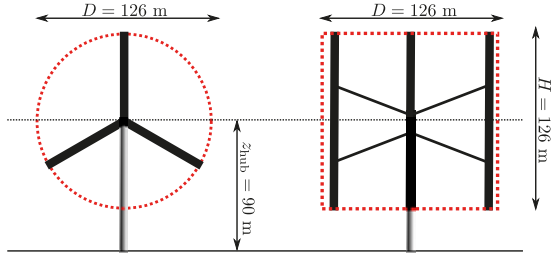

Figure 4.1. Illustration of the main characteristic dimensions of the tested turbines.

wide range of TSRs in order to identify their optimal operation where the C_P reaches its maximum value. Obtained results in figure 4.2 reveal that this occurs at $\lambda = 9.5$ and 3.5 for the HAWT and the VAWT, respectively.

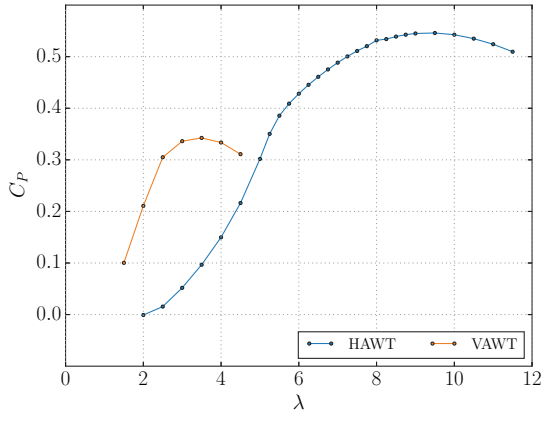

Figure 4.2. C_P as function of λ for both HAWT and VAWT.

The tested turbines have been operated in different terrains, with different surface roughnesses z_0, such that the velocity at the hub is $V_\infty = 7.83$ m/s. The lift and drag coefficients have been taken from the NREL technical report [72] and the XFOIL program [64] for the HAWT and VAWT, respectively. The inflow boundary condition was obtained by using the recycling method approach for a fully developed ABL flow over a flat terrain. The domain has a dimension of $35D \times 10D \times 5D$ (in the x, y and z directions, respectively) ensuring a proper development of the ABL flow and the resulting wake, and avoiding effects produced by the flow blockage. In order to assure the correct implementation of the recycling method, the recycling plane has been located at a distance of $15D$ from the inlet boundary, followed by the turbine rotor middle plane at $5D$ downstream. A region of $2D \times 2D \times 16D$ with local refinement is placed around and behind the turbine in order to capture the details of the resulting flow as it is displayed in figure 4.3. The whole domain is discretized using uniform hexahedral cells of 4 m and 2 m for the refined region.

Figure 4.4 shows the obtained inlet velocity profiles generated by the ALM. These numerical profiles have been compared against the profiles from the logarithmic wind shear equation, considering in both cases $V_\infty = 7.83$ m/s at the hub, for the different terrains tested. It can be noticed a good agreement for all the cases.

Figure 4.5 reveals the numerical instantaneous streamwise velocity at the vertical plane for the HAWT and the VAWT in the different terrains tested. It can be identified the wake location and geometry including the vertical shrinking for the VAWT cases and the region where the wake breaks for starting the recovery process. The larger is the atmospheric turbulence (domain surface

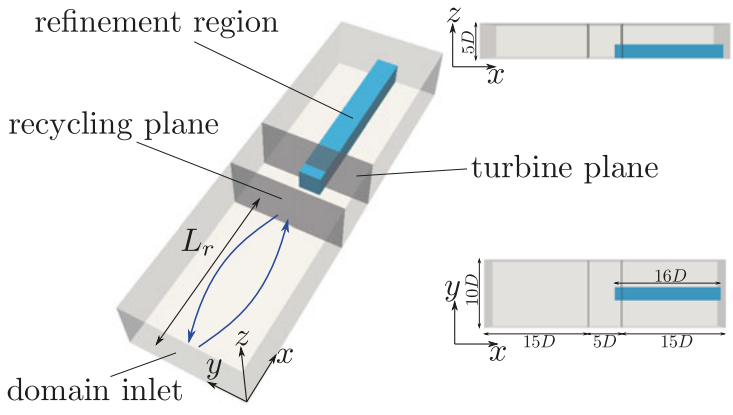

Figure 4.3. Schematic views of the domain and relevant dimensions for the implementation of the recycling method: perspective (left), lateral (upper right) and top (lower right).

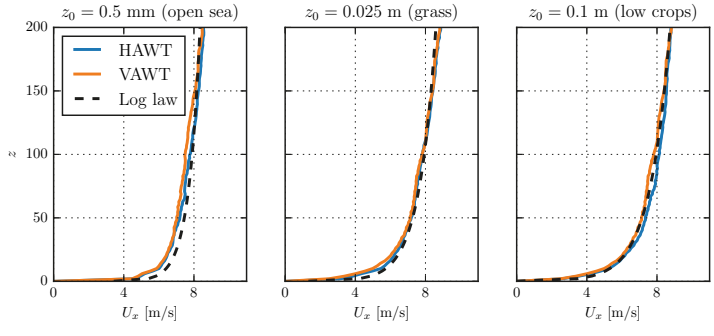

Figure 4.4. Vertical profiles of the mean streamwise velocity for the inflow conditions.

roughness) the shorter is the wake in the spanwise direction. The VAWT cases result in a bigger flow obstruction by the turbine.

The normalized mean streamwise velocity on the vertical plane and in representative sections perpendicular to the main flow are depicted in figures 4.6 and 4.7, respectively, for all the different atmospheric turbulences tested. In all the cases the resulting wake does not differs considerably in shape (geometry) and position for the same type of turbine. The location where the recovery process starts is clearly identified. Generally, larger turbulence levels lead to a faster wake recovery due to the improvement in the mixing process and momentum transfer resulting in a shorter wake in the streamwise direction. An asymmetric wake behavior is present for the VAWT which can be produced by the big difference between the velocity of the incoming flow in $x-$direction and the blade moving in the opposite upwind direction (negative

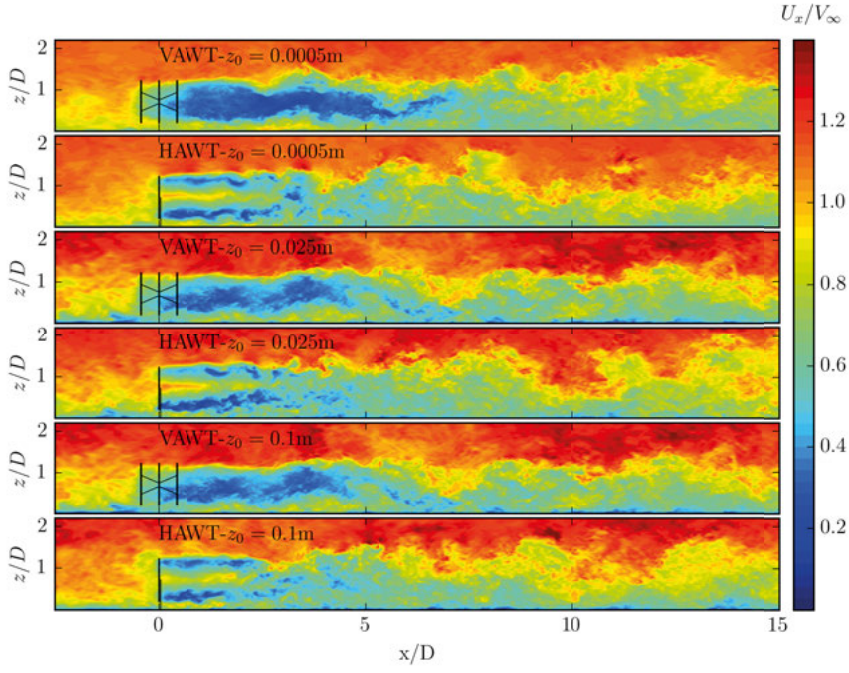

Figure 4.5. Normalized instantaneous streamwise velocity in the vertical plane at the center of the turbine for different terrains.

$x-$direction). This asymmetry of the wake is affected and amplified by its interaction with the ground.

Table 4.1 shows the aerodynamic performance of the turbines when the surface roughness length is varied. As expected, bigger power coefficient values are achieved by the HAWT in all the tested cases. However, it is noticed that the performance of HAWT is considerably affected by the atmospheric turbulence showing that larger surface roughness gives lower extracted power from the wind C_P, which is coherent with previous results documented in [73–76] where C_P values decrease when the HAWTs are operating within flows with wind speeds close to the rated one of the turbine. For the VAWT cases, a minor influence in the obtained C_P is noticed (almost constant) when varying the atmospheric turbulence. Similar results were obtained in the experimental work carried out by Möllerström et al. [77] which showed an slightly improvement in the obtained C_P at higher atmospheric turbulence levels, proposing that the H-rotor type VAWT is an appropriate device for energy extraction at sites with turbulent winds.

Horizontal and vertical profiles of normalized mean streamwise velocity components in representative sections within the wake have been used to do a quantitative comparison of the resulting wake produced by the different studied turbines and terrains. The results are shown in figure 4.8, the comparison is

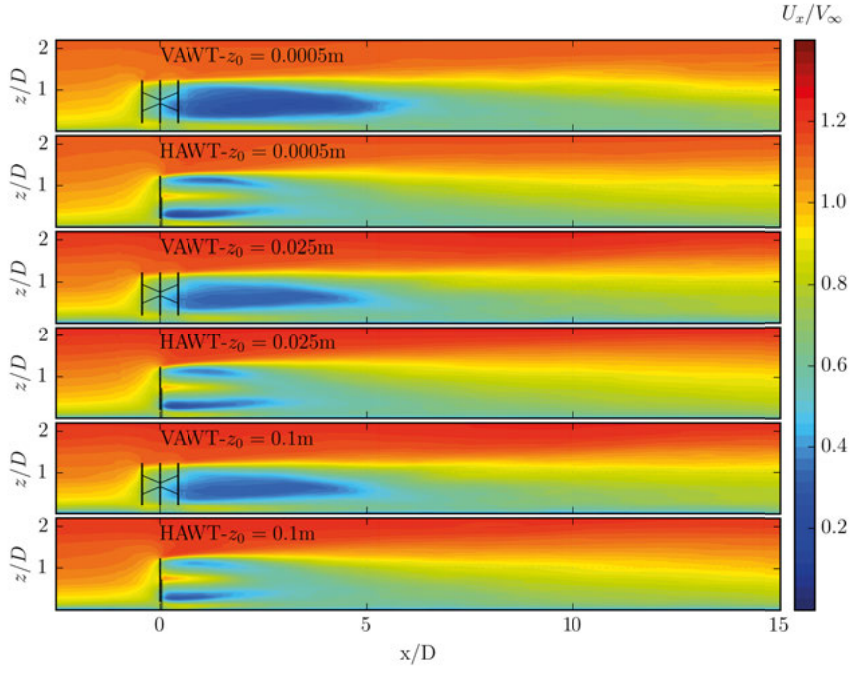

Figure 4.6. Normalized instantaneous streamwise velocity in the vertical plane at the center of the turbine for different terrains.

made with respect to the wind profile at the inlet of the domain for the different cases. The resulting wake for the HAWT cases is almost horizontally axisymmetric with the turbine axis, the region close to the rotor the velocity profiles is characterized by an irregular shape which is dissipated along the downwind sections into a smoothly Gaussian profile distribution due to the increasing mixing process, while the wake produced by the VAWT is concentrated in the central region of both vertical and horizontal profiles. A strong influence made by the ground is observed in the vertical velocity profiles. Discrepancies between the velocity deficit of both HAWT and VAWT are not considerable after the sections $x/D > 7$ where the direct contribution from the rotors are dissipated by the turbulent structures.

Table 4.1. *Aerodynamic performance of the tested turbines for the different terrains*

z_0[m]	turbine	C_P	P[MW]	C_T	T [MN]
0.0005	VAWT	0.346	1.579	0.688	0.402
	HAWT	0.558	2.003	0.870	0.399
0.025	VAWT	0.338	1.546	0.673	0.393
	HAWT	0.556	1.997	0.860	0.394
0.1	VAWT	0.338	1.546	0.673	0.393
	HAWT	0.496	1.780	0.761	0.348

4.2 Improving Farm Efficiency of Interacting Vertical Axis Wind Turbines Through Wake Deflection Using Pitched Struts

The same scaled model turbine described in section 4.1 has been employed to study the obtained performance and the resulting flow pattern from two interacting VAWTs under the influence of a deflected wake produced by a pitch angle of the struts in the upwind turbine. The configuration of this study consists of two aligned VAWTs which have a distance of $6D$ between the rotors in the direction of the main freestream flow in such a way that the area projection of the upwind turbine covers completely to the downwind one. The struts of the upwind turbine were pitched deflecting the wake while both turbines are operating in their optimal TSR. Additional tests were made in the same conditions but with offsets of $0.5D$ and $1D$ in the lateral direction. An illustration of the mentioned tests is depicted in figure 4.9. The upwind and downwind turbines are further denoted in this section as T_1 and T_2, respectively. In order to simplify the analysis of the results, a Cartesian coordinate system has been established at the location of the upwind turbine with the origin at its tower base center such that the freestream flow is in the $x-$direction.

For all the studied cases, T_1 is operating at its optimal TSR of $\lambda_1 = 3.5$ (when the struts are not pitched, $\alpha_p = 0°$). At this condition, its achieved power coefficient is $C_{P1} = 0.344$. The inflow boundary condition is a logarithmic wind shear such that the freestream velocity at the hub height ($z_{\text{ref}} = 120$ m) is equal to $V_\infty = 10$ m/s and it is defined by the log law as it was expressed in equation 2.43. The lift and drag coefficients from the XFOIL program [64] were employed for these cases.

Before studying the effects of pitching the struts on the upwind turbine T_1, the peak performance of the downwind turbine T_2 is identified when this operates within the wake from the upwind rotor for both in-line and offset configurations. Note that C_{P2} is normalized against V_∞ while the actual local velocity is less. Figure 4.10 displays the obtained power coefficient curves of T_2 under the mentioned conditions. Is is observed that the peak values occur at $\lambda_2 = 2.0, 2.5$ and 3.5 for the in-line, $0.5D-$offset and $1D-$offset cases, respectively. Obtained values of C_{P2} for the offset cases are higher over the whole range of studied TSRs, specially in the $1D-$offset case where the peak value is almost two and a half times bigger than for the other cases.

Figure 4.11 shows the normalized streamwise velocity components in the equatorial plane for both in-line and offset configurations. It can be noticed that there is a higher amount of kinetic energy available for T_2 in the offset cases since the turbine is not operating in the core of the wake which is characterized by the larger velocity deficit (color blue), this explains the higher C_{P2} obtained compared with the ones from the in-line case. There is not a considerable variation on the general structure of the wake for both in-line and $0.5D-$offset cases besides the lateral expansion in the turbine offset loca-

tion ($x/D = 6$), while a differentiable resulting wake characterized by a lower velocity deficit is obtained for the $1D-$offset case.

4.2.1 Wake deflection

The power coefficient curves of the modeled turbines when varying the pitch angle of the struts of the upwind turbine T_1 are displayed in the figure 4.12. In both in-line and $0.5D-$offset configurations there is an improvement on the extracted power of T_2 by the effects of the deflected wake. The magnitude of the improvement (difference between minimum and maximum obtained value) is more pronounced for the in-line case. For the $1D-$offset case, the power coefficients of both T_1 and T_2 are similar when there is no deflected way, and then, C_{P2} decreases when the wake in deflected in the negative direction (negative α_p) while keeps almost constant for positive pitched struts. Therefore, this is the only tested case where there is not a recognizable improvement achieved by the pitched struts mechanism. The upwind turbine T_1 does not suffer any considerable decay of its absorbed power by the pitched struts and, actually, has a small increase of the C_{P1} peak at $\alpha_p = -6$. There is an asymmetric behavior on the response to the variation of the pitched strut angles α_p. For the in-line case a better performance improvement is reached with the wake deflected pointing vertically down (negative α_p), while in the offset configuration this happens in the opposite direction.

Figures 4.13 and 4.14 show the normalized streamwise velocity field in three representative sections: the vertical middle plane through the rotor ($y/D = 0$) and the sections perpendicular to the main flow located two diameters behind the rotors of both T_1 and T_2 ($x/D = 4$ and $x/D = 10$, respectively). The wake produced by T_1 is vertically deflected allowing the main flow to (partially) penetrate into the downwind rotor of T_2, and therefore, increasing its kinetic energy available for power extraction. A larger pitch angle of the struts give a more pronounced wake deflection. A wider area is affected by using pitched struts but with lower levels of velocity deficit, producing a lateral expansion and vertical shrinking of the wake. The resulting interacting wake changes considerably between both cases when the pitched struts are applied. For the $1D-$offset case, it is noticed that the wake deflection effects are not that evident as in the other cases. When the downwind turbine is not located behind the upwind turbine, the wake expansion is not relevant even when the wake is deflected.

Discussions

- The main effect produced by the pitched struts on the wake is its expansion in the lateral direction which is compensated (for the conservation momentum) with lower levels of the velocity deficit, therefore, there is more kinetic energy available for downwind turbines.

- For the studied cases with a dual turbine configuration, the best efficiency occurs for the $1D-$offset configuration without pitched struts on T_1. Therefore, the pitched blade mechanism can improve the overall performance of interacting turbines when the downwind turbine is located within (close) the core of the wake (region with high velocity deficit). If the downwind turbine operates in the outer region of the wake, the system performance can be affected by the pitched struts since the interacting wake covers a wider area giving less kinetic energy available in the location of the downwind turbine. However, this can not be claimed as a general statement.
- As it is known, the main contribution for the extracted power by a VAWT is in the first half revolution of the rotor (upwind side) and the kinetic energy extraction occurs mostly through the blades. Hence, since the struts operate within the rotor without disturbing the incoming flow their contribution is not important for the performance of the turbine, but they can significantly modify the direction of the produced wake by varying the pitched struts angle producing power losses that can be neglected.
- Even considering the pitched struts as a novel mechanism for improving the overall performance of a VAWTs facility, several tests are required to establish its fundamentals. Among them, studies of the influence of the terrain, wind shear, geometry (aspect ratio), atmospheric boundary layer (ABL), another offset distances, etc. can be mentioned.
- The presented ALM does not consider the struts-blade joint effects, therefore, it is expected to have a variation in the obtained results in case they were implemented.
- In practice, a trailing edge flap can be implemented on the struts of operating VAWTs since there is no need to have pitched struts in both directions for a (considerably) better improvement.
- The best performance of interacting VAWTs is achieved by an appropriate spacing arrangement (among other) and it will never be surpassed by the fact of using pitched struts, however, this mechanism can considerably mitigate the losses when the incoming wind changes direction and obstructs the kinetic energy available for the downstream turbines.

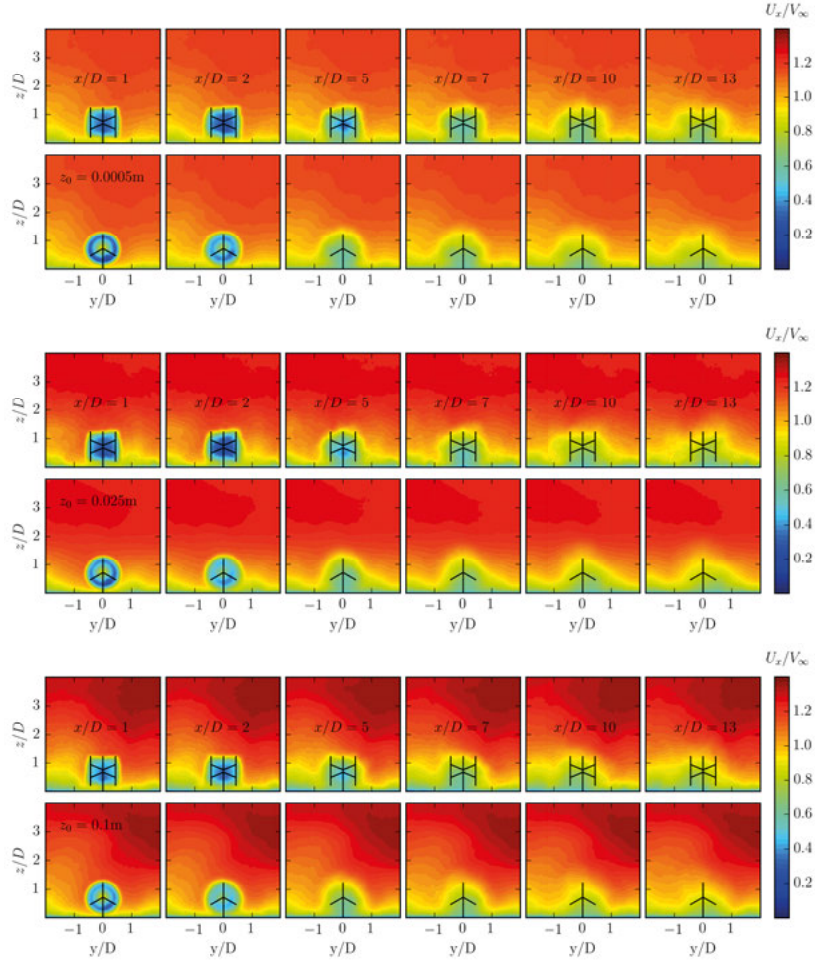

Figure 4.7. Normalized streamwise velocity at different representative sections perpendicular to the flow for different terrains with $z_0 = 0.1$ m (top), 0.025 m (center) and 0.1 m (bottom)

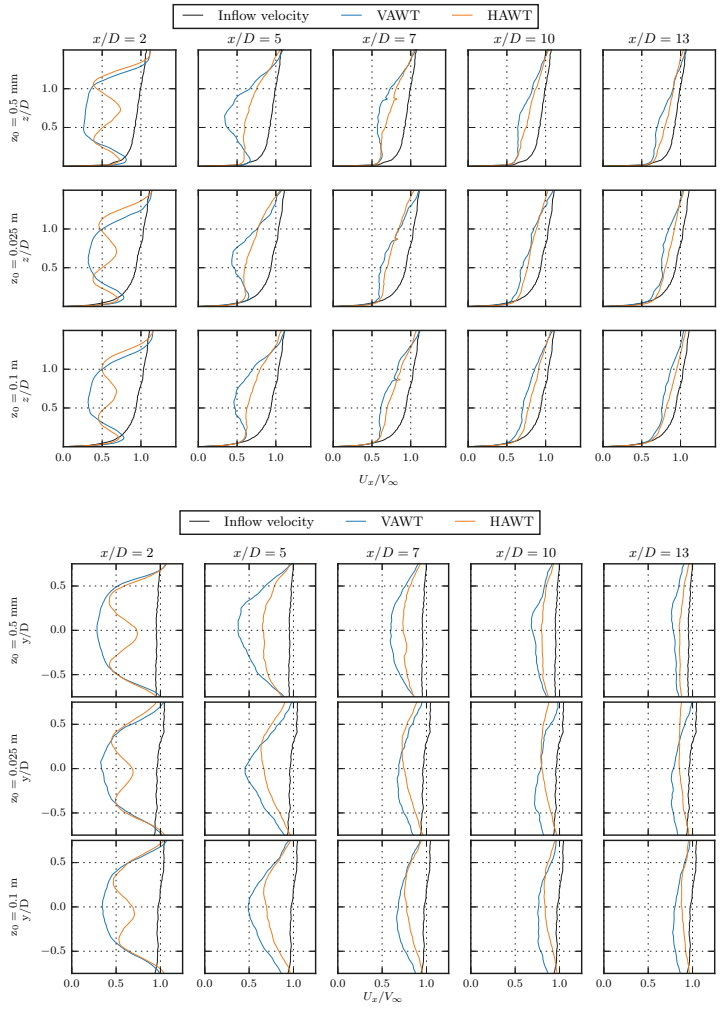

Figure 4.8. Vertical (up) and horizontal (down) profiles of the normalized velocity of the spanwise profiles of the normalized mean streamwise velocity at different representative downstream sections

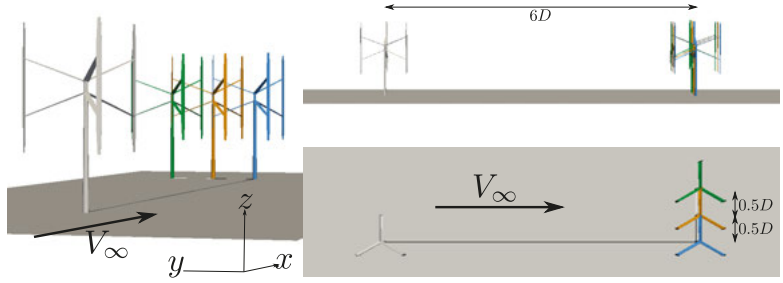

Figure 4.9. Schematic views of the domain and test configuration: from a perspective (left), upper part (top) and the side (bottom). The blue and orange turbines represent the in-line and with offset configuration cases, respectively.

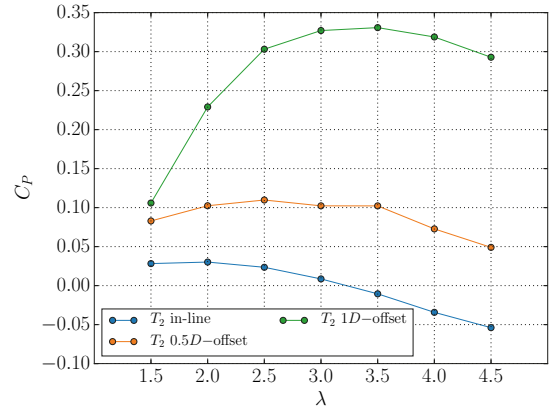

Figure 4.10. Power coefficient curves of T_2 for in-line and offset cases.

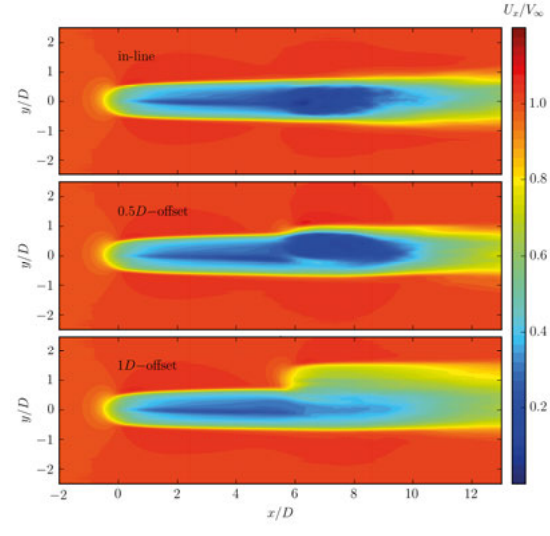

Figure 4.11. Normalized mean streamwise velocity at the horizontal equatorial plane for in-line and offset cases.

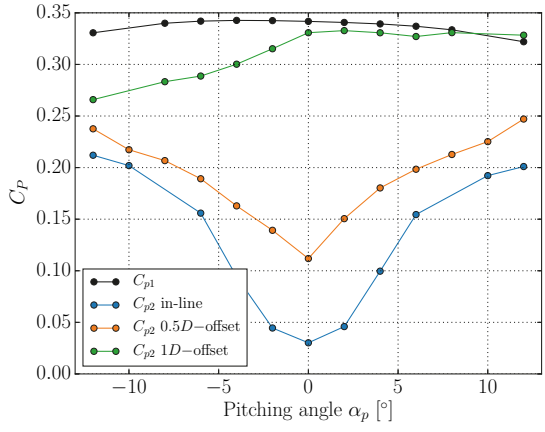

Figure 4.12. Power coefficient curves of T_2 for in-line and offset cases.

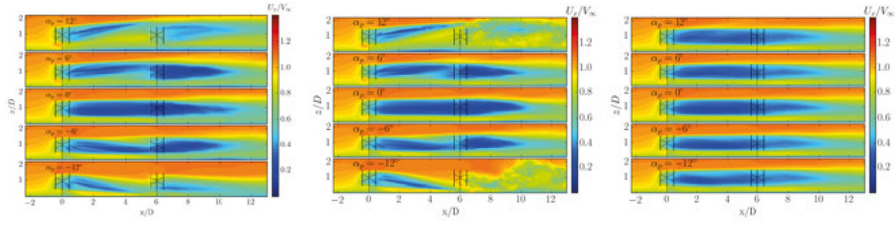

Figure 4.13. Normalized mean streamwise velocity at the vertical middle plane varying the pitched struts angle for for the in-line (left), 0.5D−offset (middle) and 1D−offset (right) cases.

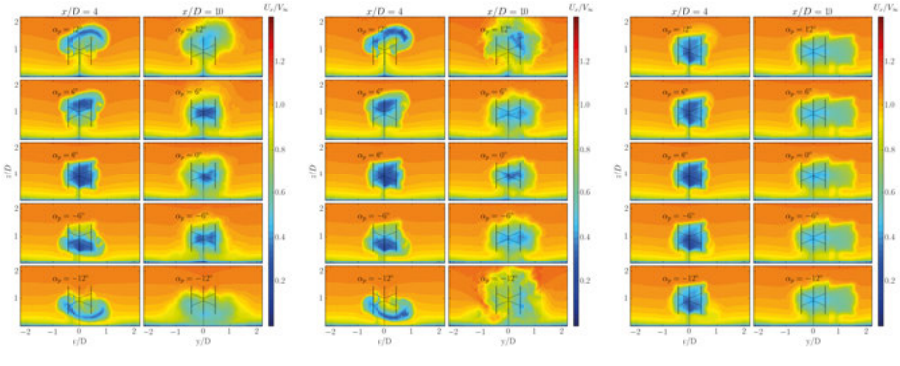

Figure 4.14. Normalized mean streamwise velocity at the representative perpendicular sections varying the pitched struts angle the in-line (left), 0.5D−offset (middle) and 1D−offset (right) cases.

5. Conclusions

This thesis addresses the complex and unsteady aerodynamics characterized by the operation of VAWTs using an actuator line model for this purpose. From the work carried out here, the author can conclude that:

- The employed actuator line model is able to reproduce and evaluate the main phenomena involved of the flow pattern of VAWTs as the resulting wake (including all its main characteristics like location, size, geometry, main vortical structures, etc.), acting forces on the different components of the devices and the performance achieved by the turbines.
- The model has been validated against experimental measurements for a wide range of tested cases with different operating condition, configurations and environments. Even considering that the numerical results don't fit perfectly with the experimental values, there is a reasonable good agreement between them. Discrepancies can be due to, among others, the accuracy in the experimental data available, a non proper description to reproduce the tested cases, the need of more detailed input data for the lift and drag coefficients, the need of an improvement of the DSM for representing the dynamic stall effects, etc.
- The employed ALM is not considerably influenced by the input data of the lift and drag coefficients for a proper representation of the normal forces on blades. The model was tested using two different sources of data showing a good agreement with experimental measurements for both sources. On the contrary, for the prediction of the power coefficient curves C_P, the simulations have notable discrepancies with measurements for one of the input coefficients employed. This can be related to an inadequate prediction and projection of the drag forces.
- It is needed to improve the representation of the vorticity released from the blade tips. The model is missing some effects of the vertical wake shrinking produced by the mentioned vorticity.
- An improvement of the DSM is required since the model loses some accuracy in the tested cases operating in the deep stall regime (i.e. low TSRs).
- The model showed numerical stability during the simulations for all the tested cases, independently of the type of turbine, operational conditions (regimes), environments and configurations.
- A HAWT and a VAWT have been compared in different ABL flows, where the wake of the VAWT is stronger in the near field. The performance of the VAWT is less sensitive to the variation of the atmospheric

turbulence. For all the tested cases, the wake becomes shorter with increasing turbulence levels.

- If two interacting turbines are totally aligned (one turbine is directly behind another turbine) it is possible to have a considerable improvement in the overall performance by using the pitched struts to deflect the wake.

6. Future Work

This chapter presents a brief overview of potential future works for both ongoing projects and new ideas.

- The current version of the used ALM considers the actuator line elements only as straight lines, which prohibits the use of it for the simulation of turbines with curved blades i.e. Darrieus type. Additional coding is required for implementing this option with the necessary considerations of curved blade effects and blade-tower joints.
- Since the model is restricted to fixed rotors, the implementation of moving turbines can be an interesting application to simulate, for example, floating turbines in offshore conditions where the rotor suffers a pseudo-periodical vertical oscillation. Moreover, the method should be coupled to a mechanical model to allow aeroelastic simulations.
- The improvement on the DSM in order to reproduce with better accuracy the effects of medium and deep stall at low TSRs.
- The implementation of the recycling method to generate stable and unstable ABL flows.
- Numerical studies of the wake deflection mechanism within ABL flows.
- Study cases for more directions of the wake deflection.
- Numerical studies of stand-alone and interacting VAWTs considering several offset arrangements (wind farms).
- Deeper studies of large scale VAWTs with different configurations of: blade profiles, geometry (aspect ratio), blade pitch angle, struts pitch angle, tower size, etc.

7. Summary of papers

This chapter presents a short summary of the papers included in this thesis.

Paper I

Validation of an Actuator Line Model Coupled to a Dynamic Stall Model for Pitching Motions Characteristic to Vertical Axis Turbines

An ALM was employed for simulating the blade loads and body forces of a pitching airfoil with periodic motions similar to those of the blades of an H-rotor type VAWT. The results have been validated against experimental results that were carried out at Glasgow University. The model has been tested for a wide range of pitching amplitudes, and therefore, with different stall conditions (none, shallow, and deep stall) showing a good agreement in general with the measurements. The author has run all the simulations, obtained the results and has written most of the article.

Paper II

Wake Flow Simulation of a Vertical Axis Wind Turbine Under the Influence of Wind Shear

A study of the resulting wake by a VAWT and how it is affected by the roughness of the terrain (without considering the atmospheric turbulence) has been carried out using the ALM. An operational H-rotor VAWT model was tested for which experimental measurements has been performed at an open site in North Uppsala (Sweden). Different surface terrains with the reference velocity at the hub have been evaluated. The model was able to reproduce the interaction between the resulting wake and the ground, and its contribution in the mixing process and the transition to the turbulent regime (identification of the wake breaking). Numerical results were validated using experimental data of normal forces, showing reasonable agreement. The author has run all the simulations, obtained the results and has written most of the article.

Paper III

Near-Wake Flow Simulation of a Vertical Axis Turbine Using an Actuator Line Model

The near wake produced by an operational H-shaped VAWT was simulated using the ALM for validating and evaluating its accuracy. The experimental activity has been performed at the Open Jet Facility (OJF) of TU Delft. First, the sensitivity of the model to the variation in the mesh resolution and temporal discretization was studied. Additionally, the performance of three different LES turbulence models were tested: Smagorisnky, dynamic k-equation and dynamic Lagrangian equation, without showing any relevant difference between them. In general, the simulated results have good agreement with measured values of velocity and vorticity in representative sections. Additional tests for studying the influence of the struts and tower were carried out showing that the main contribution on the general wake structure is made by the blades. The obtained results can be used as a reference practice guideline for choosing the propers parameters of the ALM for simulating VAWTs. The author has run all the simulations, obtained the results and has written most of the article.

Paper IV

Validation of an Actuator Line and Vortex Model using Normal Forces Measurements of a Straight-Bladed Vertical Axis Wind Turbine

A 3D ALM has been compared against a 2D and a 3D vortex model and they are validated using the normal force measurements on the blade of an operating 12 kW VAWT which is placed in North Uppsala at an open site. First, both models simulate the power coefficient curve of the device, which has been compared against the experimental one. Later, a wide range of TSRs covering from the shallow to the deep stall regime was investigated. In general, the models present a reasonable good agreement with experimental data in terms of the trend, magnitude and amplitude of the predicted forces. The ALM showed a slightly better performance representing the normal forces while the vortex model performs better for the simulation of the power coefficient curve. The author has run all the simulations with the ALM, obtained the results and has written most of the article.

Paper V

Performance and Wake Comparison of Horizontal and Vertical Axis Wind Turbines Under the Influence of the Atmospheric Boundary Layer

A numerical study of the influence of the ABL on large scale wind turbine is presented. Both a HAWT and a VAWT were tested operating stand-alone within a neutrally-stratified ABL. Three different terrains (surface roughnesses) have been considered. The main goal is to evaluate the performance of the turbines when they are operating at their optimal TSR and how it is influenced by the variation of the atmospheric turbulence, and also, to reproduce the most relevant characteristics of the resulting flow pattern. Additionally, similarities and differences between both types of turbines when they are operating at the same inflow conditions. The recycling method has been implemented to produce the fully developed ABL flow profiles. The model is previously validated using measurements of the wake and power coefficient curves of two interacting turbines within a wind tunnel and and then used to study the wake structure of both large scale HAWT and VAWT within a ABL flow. Also, a preliminary study was carried out to evaluate the difference on the blade forces of a VAWT produced by a wind shear and the ABL. The author has run all the simulations, obtained the results and has written most of the article.

Paper VI

Improving Farm Efficiency of Interacting Vertical Axis Wind Turbines Through Wake Deflection Using Pitched Struts

This work presents a numerical study of the flow field pattern and the achieved performance of two interacting in-line VAWTs. Additionally, the influence of a deflected wake produced by the pitched struts of the upstream turbine has been investigated and it is introduced as a novel mechanism for improving the performance of interacting VAWTs. The original configuration consists of two VAWTs aligned in the direction of the freestream flow. A wide range of pitched strut angles have been studied. The main goal was to quantify the influence of the wake deflection on the interacting turbines performance while they operate at the optimal TSR and in the resulting interacting flow pattern. Additionally, modified configurations with offsets have been also investigated to evaluate their contribution on the performance of the whole system. A preliminary study to identify the optimal TSR of both the upwind and downwind turbines has been carried out. The author has run all the simulations, obtained the results and has written most of the article.

8. Acknowledgements

First and foremost I would like to thank my parents, Ricardo & Inelia, I wish I have the ability to deliver love like you do.

Thanks to my beloved Franco and Ruthy. I did not choose you for being next to me forever, it was a coincidence... I am rich because of this.

Thanks to the Verburgh family and Mémé, Nico, Lyvain, Marc & Esther for making me feel at home. The distance with my Chilean family has been shorter because of the amount and quality of your love.

Thanks to my family in Chile and abroad. To Pauly, Karli, Lucas, Carola, Tía Vicky and Sra. María. You are an inexhaustible source of love, joy and dedication with me.

Thanks to my good friends in Chile, Spain and France. My 'I'll be back' sometimes take months... years... but anyway your hearts (and your houses) are always opened for me as if it had been yesterday the last time we shared.

Thanks to Enrique Carrasco & Lena Gröndahl for sharing with me and Goedele the best of you all the time, you are a treasure.

Thanks to Ricardo Fuentes and his family. I was looking for a thesis mentor... see how we ended up!

Thanks to my supervisors, Anders Goude and professor Hans Bernhoff, for all your support, trust and freedom.

Thanks to professor Mats Leijon for running the Division. I am glad to be part of it. Thanks for your efforts which allow us to be focused on the research.

Thanks to all my colleagues, ex-colleagues and friends at the Division. Especially Eduard, Oscar, José, Tobias, Dana, Andre, Aya, Dalina, Maria, Wei, Arvin, Muzaffar, Lucie, Juan, Anke, Tania, Henry, Per, Vincent, Pauline, Patrice, Johan A., Valeria, Saman and Marianna... the cold, long and dark winters are not real because of you.

Thanks to Flore, Francisco, Johan (A.K.A. JFF) and Kaspars for taking care of me in such a special way. All of you are unique... I have no words to express my gratitude.

Thanks to Prof. Hana Barankova and Prof. Ladislav Bardos for giving me the opportunity to be part of the Division and for leading me during the first years of my PhD studies.

Thanks to Uppsala University and STandUP for Energy for their financial support to this project. Also, my sincere gratitude to Anna Maria Lundins Foundation for financing my conference trips and my guest researcher internship at TU Delft, Netherlands.

Thanks to Carlos S. Ferreira and my colleagues of the Wind Energy Group at TU Delft for the valuable period with you as a guest researcher. There is a pre and post stage on my research because of you.

Thanks to my Master supervisor at University of Valladolid in Spain, Teresa Parra, who has given me permanent courage and support.

Thanks to Ingrid Ringård, Jorgen Öllson and Maria Nordengren for your indispensable support.

Thanks to all the people in Sweden who have made my stay here very happy.

Thanks to Anders Goude for your good will, great dedication and admirable skill to deliver so much knowledge in the most entertaining and disinterested way... really thanks.

And of course, thanks so much to my beloved Goedele Verburgh. I deeply love you and admire you... Sometimes it is not easy to distinguish real life from fantasy.

9. Svensk sammanfattning

De flesta vindkraftverk i drift är horisontalaxlade. Det finns emellertid ett förnyat intresse för turbiner med vertikal axel för offshore applikationer, eftersom de har flera relevanta fördelar jämfört med konventionella horisontalaxlade turbiner. Designen gör det möjligt för dem att absorbera vinden från alla riktningar, vilket förenklar den mekaniska konstruktionen, eftersom det inte finns något behov av varken girmekanism eller bladvridningsmekanism (pitch). Denna egenskap har stor fördel i offshore-miljöer, där drift och underhållskostnader har ett stort bidrag till den totala kostnaden för energigenereringen. En annan fördel med vertikalaxlade vindkraftverk är att den elektriska generatorn kan placeras vid havsnivå vilket minskar komplexiteten hos installationen och underhållet av turbinen. Detta bidrar också till stabiliteten hos hela strukturen, vilket minskar storleken och kostnaden för fundament. Detta minskar också kraven på generatorns storlek och vikt, vilket möjliggör installation av tunga direktdrivna generatorer med permanentmagneter. Vertikalaxlade vindkraftverk kännetecknas emellertid av en komplex och dynamisk strömningsmekanik som uppvisar stora utmaningar både vid experimentella mätningar såväl som för numeriska simuleringar.

Denna avhandling handlar om strämningsmekaniken för ett vertikalaxlat vindkraftverk. Huvudfokus ligger på beskrivning av de mest relevanta fenomenen som orsakar flödesbildent, vakens, belastningar på de olika komponenterna i turbinen och rotorns prestanda. Metoden "actuator line model" (ALM) använts för att uppnå detta ändamål.

De numeriska beräkningarna har validerats genom att jämföra de numeriska resultaten med mätningar för ett antal experiment under olika driftsförhållanden som har utförts i vindtunnlar, samt på en testanläggning placerad på ett öppet fält. Numeriska simuleringar har genomförts för ett stort intervall av löptal och omfattar på så sätt driftförhållanden från låga anfallsvinklar till djup överstegring (stall). Detta sista fall kräver användning av en dynamisk överstegringmodell för realistisk beräkning av de varierande krafterna på turbinbladen. Olika inkommande flödesförhållanden har också studerats, såsom likformiga logaritmiska vindflöden och flöden med ett atmosfäriskt gränsskikt. Den så kallade "recycling method" tekniken använts för att det fullt utvecklade atmosfäriska gränsskiktet. Dessutom har interaktionen mellan vindkraftverk studerats.

Modellen användes senare för att utföra två numeriska studier för storskaliga vindkraftverk. Först studerades prestanda och hastighetsfältet från ett horisontalaxlat och ett vertikalaxlat vindkraftverk när båda roterade med sina optimala

löptal under samma atmosfäriska gränsskikt. Turbulensens inverkan på flödet studerades också. Möjligheten att förbättra prestandan hos två vindkraftverk som står efter varandra undersöktes också. Detta undersöktes genom att man ändrade stigvinkeln hos bärarmarna, vilka då agerade som en fläkt och styrde undan vaken från främre vindkraftverket så den delvis missar det bakre vindkraftverket.

I allmänhet är överensstämmelsen mellan de numeriska simuleringarna och de experimentella mätningarna god, och därför får ALM anses som ett användbart verktyg för simulering av vertikalaxlade vindkraftverk. ALM betraktas som en metod med god stabilitet, bra noggrannhet och relativt låg beräkningskostnad.

10. Resumen en español

La mayoría de las turbinas eólicas en operación son del tipo de eje horizontal. Sin embargo, hay un renovado interés por las turbinas con eje vertical para aplicaciones offshore ya que éstas presentan varias ventajas relevantes sobre las turbinas convencionales de eje horizontal. La omnidireccionalidad les permite operar con el viento proveniente desde cualquier dirección, lo cual simplifica el diseño mecánico ya que no está la necesidad de un mecanismo para seguimiento del viento, ni el sistema de ajuste (pitching). Esta cualidad es altamente apreciada en ambientes offshore, en donde los costos de operación y manteniento tienen una gran contribución en el costo total de producción de energía. Otra ventaja de las turbinas de eje vertical es que el generador eléctrico puede ser ubicado a nivel de mar, lo cual reduce la complejidad de la instalación y mantención de la turbina. Esto también mejora la estabilidad de toda la estructura, y así mismo, reduce el tamaño y costo de la base (soporte), y más aún, minimiza las restricciones relacionadas al peso y tamano del generador permitiendo la instalación de pesados generadores de accionamiento directo con imanes permanentes. Sin embargo, el funcionamiento de turbinas con eje vertical es caracterizada por una mecánica de fluidos compleja y variable, la cual presenta considerables desafíos tanto como para su descripción a través de mediciones experimentales así como para simulaciones numéricas.

Esta tesis está dirigida al estudio de la aerodinámica variable envuelta inherentemente en la operación de una turbina de eje vertical. El principal foco está en la representación y entendimiento, cuantitativo y cualitativo, de los fenómenos más relevantes involucrados en el patrón de flujo resultante como puede ser la estructura general de la estela, las cargas sobre los diversos componentes de la turbina y el rendimiento del rotor. Para conseguir dicho propósito, se ha utilizado el método denominado 'actuator line model' (ALM).

Dicho modelo ha sido validado comparando los resultados numéricos con mediciones para una variada gama de experimentos con diferentes condiciones operacionales que han sido llevado a cabo dentro de túneles de viento así como también en espacios abiertos a condiciones atmosféricas. Se llevaron a cabo simulaciones numéricas considerando un amplio rango de relaciones de velocidad periférica ('tip speed ratios' o TSR en Inglés), y de esa manera, abarcar regímenes de operación con entrada en pérdida (stall) leve hasta profunda. Esta última condición demanda la implementación de un modelo de entrada en pérdida dinámica para una representación correcta de las fuerzas variables sobre los álabes de las turbinas. También han sido estudiadas diferentes condiciones de flujos de entrada como flujos uniformes, perfiles logarítmicos de

viento y flujos de la capa límite atmosférica (ABL). Para generar el flujo de la ABL completamente desarrollado se ha utilizado la técnica llamada 'recycling method'. Adicionalmente, se han estudiado la interacción entre turbinas.

Una vez que el modelo fue validado, se realizaron dos estudios numéricos para turbinas de gran escala. Primero, se evaluá el desempeño y el campo de velocidades resultante de una turbina de eje horizontal y una vertical cuando ambas están operando en su TSR óptimo expuestas al mismo flujo de la ABL. También se estudia los efectos producidos debido a la variación de la turbulencia atmosférica en el flujo. Luego, se investiga la mejora del rendimiento de dos turbinas interactuando a través de la desviación de la estela producida por la inclinación de las álabes de soporte (struts) de la turbina aguas arriba y a la vez es presentado como un mecanismo novedoso para mitigar las pérdidas en configuraciones de turbinas interactuando (por ejemplo, parque eólicos).

En general, hay buena coherencia entre los resultados numéricos y las mediciones experimentales, y por lo tanto, el ALM utilizado puede ser considerado como una potencial herramienta para la simulación de turbinas de eje vertical. El ALM se caracteriza por un costo computacional relativamente bajo, precisión en los resultados y estabilidad numérica.

References

[1] E. W. Golding, R. Harris, The generation of electricity by wind power, E. & FN Spon London, 1976.

[2] W. Commons, File:nashtifan windmills01.jpg — wikimedia commons, the free media repository, [Online; accessed 7-April-2018] (2017). URL https://commons.wikimedia.org/w/index.php?title=File:Nashtifan_Windmills01.jpg&oldid=260911921

[3] T. Ackermann, L. Söder, An overview of wind energy-status 2002, Renewable and sustainable energy reviews 6 (1-2) (2002) 67–127.

[4] W. Commons, File:brill windmill april 2017.jpg — wikimedia commons, the free media repository, [Online; accessed 7-April-2018] (2018). URL https://commons.wikimedia.org/w/index.php?title=File:Brill_windmill_April_2017.jpg&oldid=294683138

[5] R. Gasch, J. Twele, Wind power plants: fundamentals, design, construction and operation, Springer Science & Business Media, 2011.

[6] W. Commons, File:stembridgetowermill(patrickmackie)aug2006.jpg — wikimedia commons, the free media repository, [Online; accessed 7-April-2018] (2017). URL https://commons.wikimedia.org/w/index.php?title=File:StembridgeTowerMill(PatrickMackie)Aug2006.jpg&oldid=263060952

[7] W. Commons, File:amerikaanse windmolen. de alde feanen 02.jpg — wikimedia commons, the free media repository, [Online; accessed 7-April-2018] (2017). URL https://commons.wikimedia.org/w/index.php?title=File:Amerikaanse_windmolen._De_Alde_Feanen_02.JPG&oldid=242575262

[8] J. F. Manwell, J. G. McGowan, A. L. Rogers, Wind energy explained: theory, design and application, John Wiley & Sons, 2010.

[9] S. S. Johannes, Rotor adapted to be driven by wind or flowing water, uS Patent 1,697,574 (Jan. 1 1929).

[10] S. J. Savonius, Wind rotor, uS Patent 1,766,765 (Jun. 24 1930).

[11] B. F. Blackwell, R. F. Sheldahl, L. V. Feltz, Wind tunnel performance data for two-and three-bucket Savonius rotors, Sandia Laboratories Springfield, VA, USA, 1977.

[12] W. Commons, File:savonius wind turbine.jpg — wikimedia commons, the free media repository, [Online; accessed 8-April-2018] (2018). URL https://commons.wikimedia.org/w/index.php?title=File:Savonius_wind_turbine.jpg&oldid=280792998

[13] W. Commons, File:darrieus-rotor ennabeuren-3256.jpg — wikimedia commons, the free media repository, [Online; accessed 8-April-2018] (2014). URL https://commons.wikimedia.org/w/index.php?title=File:Darrieus-Rotor_Ennabeuren-3256.jpg&oldid=139431556

[14] M. Rossander, E. Dyachuk, S. Apelfröjd, K. Trolin, A. Goude, H. Bernhoff, S. Eriksson, Evaluation of a blade force measurement system for a vertical axis wind turbine using load cells, Energies 8 (6) (2015) 5973–5996.
[15] D. G. J. Marie, Turbine having its rotating shaft transverse to the flow of the current, uS Patent 1,835,018 (Dec. 8 1931).
[16] U. S. Paulsen, T. F. Pedersen, H. A. Madsen, K. Enevoldsen, P. H. Nielsen, J. Hattel, L. Zanne, L. Battisti, A. Brighenti, M. Lacaze, et al., Deepwind-an innovative wind turbine concept for offshore, European Wind Energy Association (EWEA) Annual Event.
[17] S. N. Laboratories, Offshore use of vertical-axis wind turbines gets closer look, https://share-ng.sandia.gov/news/resources/news_releases/vawts/#.WKB9WHUrKp0, accessed: 2018-04-08.
[18] D. J, First 2mw vertiwind vertical-axis prototype built, http://www.windpowermonthly.com/article/1305428/first-2mw-vertiwind-vertical-axis-prototype-built, accessed: 2018-04-08.
[19] G. Boyle, Uk offshore wind potential: How offshore wind could supply a quarter of uk electricity by 2024, Refocus 7 (4) (2006) 26–29.
[20] M. D. Esteban, J. J. Diez, J. S. López, V. Negro, Why offshore wind energy?, Renewable Energy 36 (2) (2011) 444–450.
[21] U. S. Paulsen, H. A. Madsen, J. H. Hattel, I. Baran, P. H. Nielsen, Design optimization of a 5 mw floating offshore vertical-axis wind turbine, Energy Procedia 35 (2013) 22–32.
[22] M. Borg, A. Shires, M. Collu, Offshore floating vertical axis wind turbines, dynamics modelling state of the art. part i: Aerodynamics, Renewable and Sustainable Energy Reviews 39 (2014) 1214–1225.
[23] G. Tescione, On the aerodynamics of a vertical axis wind turbine wake: An experimental and numerical study.
[24] S. Eriksson, A. Solum, M. Leijon, H. Bernhoff, Simulations and experiments on a 12 kw direct driven pm synchronous generator for wind power, Renewable Energy 33 (4) (2008) 674–681.
[25] S. A. Huyer, D. Simms, M. C. Robinson, Unsteady aerodynamics associated with a horizontal-axis wind turbine, AIAA journal 34 (7) (1996) 1410–1419.
[26] F. Bülow, J. Kjellin, S. Eriksson, M. Bergkvist, P. Ström, H. Bernhoff, Adapting a vawt with pm generator to telecom applications, in: European Wind Energy Conference & Exhibition, 2010.
[27] A. Solum, P. Deglaire, S. Eriksson, M. Stålberg, M. Leijon, H. Bernhoff, Design of a 12kw vertical axis wind turbine equipped with a direct driven pm synchronous generator, in: EWEC 2006-European wind energy conference & exhibition, Athens, Greece, 2006.
[28] J. Kjellin, F. Bülow, S. Eriksson, P. Deglaire, M. Leijon, H. Bernhoff, Power coefficient measurement on a 12 kW straight bladed vertical axis wind turbine, Renewable energy 36 (11) (2011) 3050–3053.
[29] S. Eriksson, H. Bernhoff, M. Leijon, A 225 kw direct driven pm generator adapted to a vertical axis wind turbine, Advances in Power Electronics 2011.
[30] S. Eriksson, Direct driven generators for vertical axis wind turbines, Ph.D. thesis, Acta Universitatis Upsaliensis (2008).

[31] P. Deglaire, Analytical aerodynamic simulation tools for vertical axis wind turbines, Ph.D. thesis, Acta Universitatis Upsaliensis (2010).
[32] J. Kjellin, Vertical axis wind turbines: Electrical system and experimental results, Ph.D. thesis, Acta Universitatis Upsaliensis (2012).
[33] A. Goude, Fluid mechanics of vertical axis turbines: Simulations and model development, Ph.D. thesis, Acta Universitatis Upsaliensis (2012).
[34] F. Bülow, A generator perspective on vertical axis wind turbines, Ph.D. thesis, Acta Universitatis Upsaliensis (2013).
[35] E. Dyachuk, Aerodynamics of vertical axis wind turbines: Development of simulation tools and experiments, Ph.D. thesis, Acta Universitatis Upsaliensis (2015).
[36] M. Erik, Noise, eigenfrequencies and turbulence behavior of a 200 kw h-rotor vertical axis wind turbine, Ph.D. thesis, Acta Universitatis Upsaliensis (2017).
[37] M. Rossander, Electromechanics of vertical axis wind turbines, Ph.D. thesis, Acta Universitatis Upsaliensis (2017).
[38] J. N. Sørensen, W. Z. Shen, Computation of wind turbine wakes using combined navier-stokes/actuator-line methodology, in: 1999 European Wind Energy Conference and Exhibition, 1999, pp. 156–159.
[39] J. Leishman, T. Beddoes, A generalised model for airfoil unsteady aerodynamic behaviour and dynamic stall using the indicial method, in: Proceedings of the 42nd Annual forum of the American Helicopter Society, Washington DC, 1986, pp. 243–265.
[40] W. Sheng, R. Galbraith, F. Coton, A modified dynamic stall model for low mach numbers, Journal of Solar Energy Engineering 130 (3) (2008) 031013.
[41] P. Bachant, M. Wosnik, Simulating wind and marine hydrokinetic turbines with actuator lines in rans and les, in: APS Meeting Abstracts, 2015.
[42] P. Bachant, A. Goude, M. Wosnik, Actuator line modeling of vertical-axis turbines, arXiv preprint arXiv:1605.01449.
[43] P. Bachant, A. Goude, M. Wosnik, turbinesfoam: v0.0.7, doi:/10.5281/zenodo.49422. URL `http://dx.doi.org/10.5281/zenodo.49422` (Apr. 2016).
[44] J. N. Sørensen, W. Z. Shen, Numerical modeling of wind turbine wakes, Journal of fluids engineering 124 (2) (2002) 393–399.
[45] S. Shamsoddin, F. Porté-Agel, Large eddy simulation of vertical axis wind turbine wakes, Energies 7 (2) (2014) 890–912.
[46] M. J. Churchfield, Y. Li, P. J. Moriarty, A large-eddy simulation study of wake propagation and power production in an array of tidal-current turbines, Phil. Trans. R. Soc. A 371 (1985) (2013) 20120421.
[47] W. J. McCroskey, The phenomenon of dynamic stall., Tech. rep., NATIONAL AERONUATICS AND SPACE ADMINISTRATION MOFFETT FIELD CA AMES RESEARCH CENTER (1981).
[48] E. Dyachuk, A. Goude, H. Bernhoff, Dynamic stall modeling for the conditions of vertical axis wind turbines, AIAA journal 52 (1) (2013) 72–81.
[49] P. Fraunie, C. Beguier, I. Paraschivoiu, G. Brochier, Water channel experiments of dynamic stall on darrieus wind turbine blades, Journal of Propulsion and Power 2 (5) (1986) 445–449.
[50] J. Strickland, T. Smith, K. Sun, Vortex model of the darrieus turbine: an

analytical and experimental study. final report.
[51] P. Migliore, W. Wolfe, J. Fanucci, Flow curvature effects on darrieus turbine blade aerodynamics, Journal of Energy 4 (2) (1980) 49–55.
[52] J. D. Anderson Jr, Fundamentals of aerodynamics, Tata McGraw-Hill Education, 2010.
[53] A. Silva Lopes, J. Palma, F. Castro, Simulation of the Askervein flow. Part 2: Large-eddy simulations, Boundary-Layer Meteorol. 125 (1) (2007) 85–108.
[54] M. Diebold, C. Higgins, J. Fang, A. Bechmann, M. Parlange, Flow over hills: A Large-Eddy Simulation of the Bolund case, Boundary-Layer Meteorol. 148 (1) (2013) 177–194. doi:10.1007/s10546-013-9807-0.
[55] A. Chaudhari, Large-eddy simulation of wind flows over complex terrains for wind energy applications, Ph.D. thesis, Lappeenranta University of Technology (2014).
[56] A. Chaudhari, A. Hellsten, J. Hämäläinen, Full-scale experimental validation of large-eddy simulation of wind flows over complex terrain: The bolund hill, Advances in Meteorology 2016 (2016) 14 pages, article ID 9232759. doi:10.1155/2016/923275.
[57] A. Chaudhari, V. Vuorinen, J. Hämäläinen, A. Hellsten, Large-eddy simulations for hill terrains: validation with wind-tunnel and field measurements, Computational and Applied Mathematics in-press, published online at https://doi.org/10.1007/s40314-017-0435-z.
[58] F. Porté-Agel, Y.-T. Wu, H. Lu, R. J. Conzemius, Large-eddy simulation of atmospheric boundary layer flow through wind turbines and wind farms, Journal of Wind Engineering and Industrial Aerodynamics 99 (4) (2011) 154–168.
[59] Y.-T. Wu, F. Porté-Agel, Atmospheric turbulence effects on wind-turbine wakes: An les study, energies 5 (12) (2012) 5340–5362.
[60] V. Vuorinen, A. Chaudhari, J.-P. Keskinen, Large-eddy simulation in a complex hill terrain enabled by a compact fractional step openfoam solver, Advances in Engineering Software 79 (0) (2015) 70 – 80. doi:http://dx.doi.org/10.1016/j.advengsoft.2014.09.008.
URL http://www.sciencedirect.com/science/article/pii/S0965997814001513
[61] R. Angell, P. Musgrove, R. Galbraith, U. of Glasgow. Department of Aeronautics, F. Mechanics, The Collected Data for Tests on a NACA 0021 Aerofoil, G. U. Aero report, University of Glasgow, Department of Aeronautics & Fluid Mechanics, 1988.
URL https://books.google.se/books?id=OmHVNQAACAAJ
[62] E. Dyachuk, M. Rossander, A. Goude, H. Bernhoff, Measurements of the aerodynamic normal forces on a 12-kW straight-bladed vertical axis wind turbine, Energies 8 (8) (2015) 8482–8496.
[63] R. E. Sheldahl, P. C. Klimas, Aerodynamic characteristics of seven symmetrical airfoil sections through 180-degree angle of attack for use in aerodynamic analysis of vertical axis wind turbines, Tech. rep., Sandia National Labs., Albuquerque, NM (USA) (1981).
[64] M. Drela, Xfoil: An analysis and design system for low reynolds number airfoils, in: Low Reynolds number aerodynamics, Springer, 1989, pp. 1–12.
[65] V. Mendoza, A. Goude, Wake flow simulation of a vertical axis wind turbine

under the influence of wind shear, in: Journal of Physics: Conference Series, Vol. 854, IOP Publishing, 2017, p. 012031.
[66] P. Krogstad, L. Sætran, M. S. Adaramola, 'blind test 3' calculations of the performance and wake development behind two in-line and offset model wind turbines, Journal of Fluids and Structures 52 (2015) 65–80.
[67] P. Krogstad, L. Sætran, Invitation to the 2013 'blind test 3' workshop two in-line wind turbines with spanwise offset, Department of Energy and Process Engineering, NTNU, Trondheim, Norway.
[68] S. Cakmakcioglu, I. Sert, O. Tugluk, N. Sezer-Uzol, 2-d and 3-d cfd investigation of nrel s826 airfoil at low reynolds numbers, in: Journal of Physics: Conference Series, Vol. 524, IOP Publishing, 2014, p. 012028.
[69] G. Tescione, D. Ragni, C. He, C. S. Ferreira, G. Van Bussel, Near wake flow analysis of a vertical axis wind turbine by stereoscopic particle image velocimetry, Renewable Energy 70 (2014) 47–61.
[70] P. Bachant, A. Goude, M. Wosnik, Actuator line modeling of vertical-axis turbines, arXiv preprint arXiv:1605.01449.
[71] V. Mendoza, P. Bachant, M. Wosnik, A. Goude, Validation of an actuator line model coupled to a dynamic stall model for pitching motions characteristic to vertical axis turbines, in: Journal of Physics: Conference Series, Vol. 753, IOP Publishing, 2016, p. 022043.
[72] J. Jonkman, S. Butterfield, W. Musial, G. Scott, Definition of a 5-MW reference wind turbine for offshore system development, Tech. rep., National Renewable Energy Lab.(NREL), Golden, CO (United States) (2009).
[73] A. Honrubia, A. Vigueras-Rodríguez, E. Gómez-Lázaro, The influence of turbulence and vertical wind profile in wind turbine power curve, in: Progress in turbulence and wind energy IV, Springer, 2012, pp. 251–254.
[74] K. Kaiser, W. Langreder, H. Hohlen, J. Højstrup, Turbulence correction for power curves, in: Wind Energy, Springer, 2007, pp. 159–162.
[75] R. Wagner, M. Courtney, T. J. Larsen, U. S. Paulsen, Simulation of shear and turbulence impact on wind turbine performance.
[76] J. Gottschall, J. Peinke, How to improve the estimation of power curves for wind turbines, Environmental Research Letters 3 (1) (2008) 015005.
[77] E. Möllerström, F. Ottermo, A. Goude, S. Eriksson, J. Hylander, H. Bernhoff, Turbulence influence on wind energy extraction for a medium size vertical axis wind turbine, Wind Energy 19 (11) (2016) 1963–1973.
[78] J. G. Leishman, T. Beddoes, A semi-empirical model for dynamic stall, Journal of the American Helicopter society 34 (3) (1989) 3–17.

Acta Universitatis Upsaliensis

Digital Comprehensive Summaries of Uppsala Dissertations from the Faculty of Science and Technology 1671

Editor: The Dean of the Faculty of Science and Technology

A doctoral dissertation from the Faculty of Science and Technology, Uppsala University, is usually a summary of a number of papers. A few copies of the complete dissertation are kept at major Swedish research libraries, while the summary alone is distributed internationally through the series Digital Comprehensive Summaries of Uppsala Dissertations from the Faculty of Science and Technology. (Prior to January, 2005, the series was published under the title "Comprehensive Summaries of Uppsala Dissertations from the Faculty of Science and Technology".)

Distribution: publications.uu.se
urn:nbn:se:uu:diva-348346

ACTA
UNIVERSITATIS
UPSALIENSIS
UPPSALA
2018